# Id2 GABAergic interneurons: a neglected fourth major group of cortical inhibitory cells

Robert Machold[1], Shlomo Dellal[1#], Manuel Valero[1#], Hector Zurita[1], Illya Kruglikov[1], John Meng[1,2], Jessica L. Hanson[1&], Yoshiko Hashikawa[1], Benjamin Schuman[1], György Buzsáki[1,3], Bernardo Rudy[1,3,4*]

Affiliations:

1: Neuroscience Institute, NYU School of Medicine, New York, NY, 10016
2: Center for Neural Science, NYU, New York, NY, 10003
3: Department of Neuroscience and Physiology, NYU School of Medicine, New York, NY, 10016
4: Department of Anesthesiology, Perioperative Care and Pain Medicine, NYU School of Medicine, New York, NY, 10016

# These authors contributed equally to this manuscript

& Present address: Department of Integrative Physiology and the Institute for Behavioral Genetics, University of Colorado Boulder, Boulder, CO, 80309

* Corresponding author: Bernardo.Rudy@nyulangone.org

**Summary**

Cortical GABAergic interneurons (INs) represent a diverse population of mainly locally projecting cells that provide specialized forms of inhibition to pyramidal neurons and other INs. Most recent work on INs has focused on subtypes distinguished by expression of Parvalbumin (PV), Somatostatin (SST), or Vasoactive Intestinal Peptide (VIP). However, a fourth group that includes neurogliaform cells (NGFCs) has remained enigmatic due to a lack of genetic tools. Here, we show that these INs can be accessed experimentally using intersectional genetics with the gene *Id2*. We find that outside of layer 1 (L1), the majority of Id2 INs are NGFCs that express high levels of neuropeptide Y (NPY) and exhibit a late-spiking firing pattern, with extensive local connectivity. While much sparser, non-NGFC Id2 INs had more variable properties, with most cells corresponding to a diverse group of INs that strongly expresses the neuropeptide CCK. *In vivo*, using silicon probe recordings, we observed several distinguishing aspects of NGFC activity, including a strong rebound in activity immediately following the cortical down state during NREM sleep. Our study provides insights into IN diversity and NGFC distribution and properties, and outlines an intersectional genetics approach for further study of this neglected group of INs.

## Introduction

The neocortex is comprised of two primary neuronal classes: pyramidal cells that release the excitatory neurotransmitter glutamate, and interneurons that release the inhibitory neurotransmitter GABA. Pyramidal neurons project their axons locally and distally to form extended circuit ensembles across cortical and subcortical areas, whereas GABAergic interneurons (INs) typically project their axons locally to regulate the excitability of nearby pyramidal cells and other INs. Pyramidal neurons share a common dendritic structure characterized by an apical dendrite that typically extends up towards the pial surface with extensive arborization in cortical layer 1 (L1), a cell sparse region that receives diverse long-range cortical and thalamic axonal projections (1-4). In combination with its basal dendrite and somatic inputs, the pyramidal neuron thus has the ability to distinguish and integrate inputs from bottom-up and top-down sources in real-time, a key feature that enables dynamic cortical activity and adaptability during the animal's interactions with the external world.

While the morphological diversity of IN dendrites and axons was noted over a century ago by Ramón y Cajal, recent work has begun to elucidate how this specialization of IN subtypes allows for compartment-specific inhibition across the entire pyramidal neuron (5-10). The discovery of molecular markers in tandem with electrophysical and morphological approaches has enabled the delineation of several major IN groups and subtypes, each with distinctive roles in the cortical circuit (5, 11-17). INs that express the $Ca^{2+}$ binding protein parvalbumin (PV), which account for ~40% of the GABAergic INs, exhibit fast-spiking properties, with most projecting their axons to form perisomatic baskets on nearby pyramidal neuron soma (18). In layer 4 of

41 sensory cortical areas, these PV INs form a canonical circuit in which they provide
42 feedforward inhibition of excitatory neurons receiving core thalamic inputs. A distinct but
43 less abundant subtype of PV INs are the chandelier cells, whose axons form cartridge-
44 like inputs on the pyramidal neuron axon initial segment, thereby enabling control and
45 coordination of the axonal output of pyramidal neuron ensembles (19-21). Somatostatin
46 (SST) expressing interneurons (accounting for 30% of the INs) represent a second
47 major group of INs, with the majority characterized by an ascending axonal arbor that
48 targets the distal apical dendrites of pyramidal cells (SST Martinotti cells) (5, 22). A third
49 major group of INs is distinguished by the expression of the neuropeptide vasoactive
50 intestinal peptide (VIP); these interneurons account for ~12% of the INs in the neocortex
51 and include cells that preferentially target other interneurons, particularly SST INs, and
52 thus act to disinhibit the local circuit (23-26). The vast majority of recent studies
53 exploring the roles of INs in cortical function have focused on these three groups, in no
54 small part due to the establishment of genetic tools in rodents for targeting and
55 manipulating the activity of each group (11, 27-29). This work has revealed how IN
56 diversity facilitates greater flexibility and computational power in cortical circuits.
57 In addition to the three main IN groups described above, there remains an
58 additional population of GABAergic interneurons (about 18% of the INs in the
59 neocortex) that have been much less studied. The composition of this IN population,
60 particularly enriched in superficial layers of the neocortex, includes ~90% of the INs in
61 layer 1 (5, 30) as well as neurogliaform cells (NGFCs) in all layers and “CCK basket
62 cells” (CCK BCs), two IN types previously identified in the neocortex that do not express
63 PV, SST or VIP (31-34). NGFCs are an interneuron type that exhibits several

remarkable properties, including an extremely high degree of output connectivity to other cells (pyramidal neurons and other INs) and the ability to induce postsynaptic GABA-B responses following a single action potential (35-38). CCK BCs are a rare species in the neocortex whose synapses on pyramidal neurons exhibit endocannabinoid mediated depolarization induced suppression of inhibition (DSI) (34, 39).

Here, we show that Id2 is a marker for the INs in the neocortex that do not express PV, SST or VIP, including the non-VIP cells in L1, NGFCs in L2-6 and a variety of CCK INs. Using intersectional genetic strategies to label and optogenetically stimulate Id2 INs, we find that the vast majority of Id2 INs in L2-6 are NPY-expressing NGFCs that exhibit the late-spiking firing pattern and broad connectivity characteristic of these cells. In contrast, the much rarer non-NGFC Id2 INs display diverse firing patterns and DSI but sparse local connectivity. Combining opto-tagging with *in vivo* silicon probe recordings, we describe the brain state dependence of the activity of Id2 INs, and observe several intriguing features of NGFC in vivo behavior, such as a robust rebound in activity immediately following the cortical down state. Thus, our work furthers the study of IN diversity and enables genetic access to a group of INs that despite their potent GABAergic output have remained somewhat mysterious to date.

82 **Results**

83 Cortical GABAergic INs are specified during embryogenesis in the medial and
84 caudal ganglionic eminences of the ventral telencephalon (MGE and CGE, respectively)
85 (40-42), with a fraction of non-MGE derived INs originating from the preoptic area (POA)
86 (43). All cortical PV and SST INs arise from Nkx2.1+ progenitors within the MGE (44),
87 and express Lhx6 during tangential migration and in the adult (45). Cortical CGE
88 derived INs, i.e., the non-PV, non-SST subtypes labeled in the Htr3a(BAC)-EGFP
89 mouse line (the 5HT3aR INs) (46) can be divided into two primary populations: VIP- and
90 non-VIP-expressing (5, 47). While transgenic targeting approaches for PV, SST, and
91 VIP INs have been developed and widely implemented (11, 28), accessing non-VIP
92 CGE (or 5HT3aR) INs – a fourth major IN group – has been challenging due to a lack of
93 genetic strategies to target this population, and therefore the IN subtypes present in this
94 population are not well characterized.

95 We examined cortical single-cell transcriptome data (scRNAseq) from the Allen
96 Institute (13) and observed that expression of the Id2 gene was highly enriched in the
97 INs in their collection that do not express PV, SST or VIP (Fig. 1A) (48). The Id2 IN
98 population includes cells that express markers known to be present in non-VIP CGE INs
99 such as Reelin (49), and NPY (50), as well as the more recently identified markers
100 NDNF, Lamp5 and Sncg (13). Updated and expanded cortical and hippocampal
101 scRNAseq data from the Allen Institute (17) confirms that Id2 is a useful marker for
102 studying non-PV, SST, or VIP INs (Fig. S1). To develop a transgenic approach to target
103 Id2 INs, we took advantage of an existing Id2-CreER driver line (51) that expresses a
104 tamoxifen-inducible form of Cre recombinase (52). Since Id2 is also expressed in

105 pyramidal and non-neuronal cell types in the cortex, we crossed the Id2-CreER driver
106 with a pan-IN Flp driver (Dlx5/6-Flpe) (49) such that only Id2 INs would be targeted with
107 intersectional reporters (Fig. 1B). In combination with the Cre and Flp dependent
108 tdTomato reporter Ai65 (27), this intersectional genetics approach yielded labeling of
109 INs in all cortical layers of the somatosensory cortex barrel field (S1BF) following
110 tamoxifen administration to activate the CreER (Fig. 1C).
111 **Histological analysis of Id2 INs.** To determine the proportion of Id2 vs. non-Id2 INs,
112 we utilized the intersectional/subtractive reporter FLTG (53) where Flp activity results in
113 tdTomato expression, but Flp + Cre results in EGFP labeling (Fig. 1D). Quantification of
114 Id2 INs (green) and non-Id2 INs (red) in the S1BF of well-labeled brains yielded an
115 overall fraction of 18% (680/3812 cells, n=4 brains), with the majority of Id2 INs located
116 in superficial layers (L1-3; Fig. 1E, F). This proportion and distribution was consistent
117 with our previous estimates for non-VIP 5HT3aR or CGE INs (5), indicating that this
118 genetic strategy was successful in targeting this population. We observed a similar
119 overall proportion of Id2 INs in other sensory areas (e.g., V1), consistent with a recent
120 comprehensive survey of interneuron subtype distribution (17) (Fig. S1), as well as in a
121 higher order cortical area, the prelimbic cortex (18%; Fig. S2).
122 To assess any potential overlap between Id2 INs and PV, SST, or VIP INs, we
123 performed intersectional genetic labeling experiments with the respective Flp drivers
124 that cover those populations. Both PV and SST INs originate from Nkx2.1+ progenitors
125 (i.e., MGE lineages; (44)), and are efficiently labeled using an Nkx2.1-Flpo driver line
126 (28). However, there is also a substantial population of neurogliaform INs (NGFCs) that
127 also arise from the MGE, the vast majority of which migrate to the hippocampus (54). A

128 small fraction of these MGE-derived NGFCs are observed in the neocortex; these are
129 the sparse deep layer Lamp5/Lhx6 population described and characterized previously
130 by us using intersectional genetics with Id2 (Id2-CreER; Nkx2.1-Flpo; Ai65) (55, 56).
131 Id2/Nkx2.1 cells did not show any overlap with PV or SST, and were mostly localized in
132 L6 (56) (Fig. S3). To examine possible overlap with VIP populations, we generated Id2-
133 CreR; VIP-Flpo; Ai65 animals and assessed the degree of IN labeling. Here too, we
134 observed very few labeled cells in S1BF, with most being located along the L1/2 border
135 (Fig. S3). While Id2/VIP cells were extremely sparse in S1BF, they were somewhat
136 more prevalent in the prelimbic cortex along the L1/2 border (Fig. S3). Thus, we find
137 that the vast majority of Id2 INs (>95%) are distinct from PV, SST or VIP populations,
138 and in the cortex, almost all originate from non-Nkx2.1 lineages (i.e., from the
139 CGE/POA).

140 In superficial layers (L1-3), expression of neuropeptide Y (NPY) has been utilized
141 successfully as a proxy to identify NGFCs (30, 50, 57, 58). We evaluated the overlap
142 between Id2 INs and NPY by performing fluorescence ISH (FISH) for tdTomato and
143 NPY on tissue cryosections from Id2-CreER; Dlx5/6; Ai65 brains (S1BF; Fig. 2A-B). The
144 proportion of Id2/NPY cells vs. the total Id2 labeled population in S1BF ranged from
145 29% in L1 to 82% in L2/3, 95% in L4-5, and 61% in L6, with a combined proportion in
146 L2-5 of 87% (638 cells counted, sections from three brains), suggesting that in contrast
147 to L1, where Id2 INs consist of several subtypes (30), the vast majority of Id2 cells
148 outside of L1 are NGFCs. Within L1, our findings are consistent with our previous
149 analysis that about 30% of L1 INs are NPY-expressing NGFCs (30). We further
150 confirmed that most Id2 INs are NPY-expressing throughout different sensory cortical

151 areas by generating Id2-CreER; Dlx5/6-Flpe; Ai65; NPY-hrGFP animals and comparing
152 labeling in S1BF, V1 and A1 (Fig. S4).
153 To explore the nature of the non-NPY Id2 neurons in L2-6, we examined the
154 overlap between Id2 labeled cells and relatively high levels of CCK expression as the
155 latter is a proxy for a sparse population of INs that include the large CCK basket cells
156 (59-61). Using IHC for CCK (Fig. 2C-D), overall in L2-6 of S1BF we observed that 15%
157 of Id2 labeled INs exhibited strong CCK expression (165/1123 cells, sections from three
158 brains), with Id2/CCK cells being most abundant in L2 (14% of Id2 cells) and L6 (25%).
159 Thus, a significant fraction of the Id2/non-NPY population in cortical layers outside of L1
160 appear to be CCK+ IN subtypes (~80% in L2/3).
161 **Electrophysiological and morphological properties of Id2 INs.** The molecular
162 analysis suggests that the vast majority of Id2 INs are neurogliaform cells (NGFCs). To
163 test this hypothesis, we characterized the firing properties of Id2 INs in L2-5 of S1BF in
164 acute brain slices. The cells were filled with biocytin during electrophysiological recording
165 for post-hoc morphological analysis. NGFCs in L2/3 and L1 have been shown to have a
166 late-spiking (LS) firing pattern characterized by delayed firing following a slow ramp
167 depolarization when depolarized with step current injections to near-threshold membrane
168 potentials (5, 30, 35, 37, 38). NGFCs in these layers were also found to fire spike trains
169 with little spike frequency adaptation, or even spike frequency acceleration, during
170 depolarizations close to threshold, and mild adaptation during suprathreshold
171 depolarizations. Action potentials in NGFCs have a large AHP and a slow ADP (30, 35,
172 37, 62-64). We found that in a sample of randomly recorded Id2 cells (n=76), the large
173 majority in L2-5 had a LS firing pattern (36/45; 80% in L2/3 and 28/31; 90% in L4-L5)

174 (Figure 3). These proportions are similar to the proportion of Id2/NPY cells (Fig. 2). The
175 Id2 LS cells also showed weak spike frequency adaptation during near threshold
176 membrane depolarizations and had other electrophysiological properties typical of
177 NGFCs (Table 1).

178 Morphologically, the LS cells in L2-5 had the characteristic features of NGFCs with
179 short multipolar dendrites emanating around the cell body and a significantly larger, dense
180 axonal arbor surrounding the cell body and dendritic arbor (Figure 3A-B and S5; n=15),
181 consistent with previous descriptions of NGFC in these layers across several neocortical
182 areas (35-38, 64). NGFCs in L1 resemble NGFCs in L2-5 in having short dendrites and
183 dense axonal arborization, but their axonal arbor extends for longer horizontal distances,
184 spanning several columns (9, 10, 30, 62, 65, 66) and have been called ‘‘elongated
185 neurogliaform cells’’ (9, 10). We found that in the LS cells in deeper layers, the axonal
186 arbor was also asymmetrical, often extending in the vertical (columnar) direction. These
187 differences between NGFCs across cortical layers are also evident in the NGFC
188 morphologies illustrated in a recent patch-seq study (16). The remaining Id2 cells (20%
189 in L2/3 and 10% in L4-5) had either an irregular or a bursting firing pattern during low to
190 moderate depolarizations (Fig. 3C , 3D, 3F, and Table 1) and narrower action potentials
191 (Fig. 3E). We also observed that a small minority of the non-LS Id2 cells in L2/3 (~15%)
192 were likely alpha-7 cells, a L1 Id2 interneuron subtype typically localized in the deeper
193 part of L1, which has a bursting firing pattern that can be distinguished from other L2/3
194 bursting cells by the properties of the burst, significantly lower input resistance, and
195 morphology (Fig. S5) (30).

196 The histological analysis showed that the majority (~80% in L2/3) of the non-NPY
197 Id2 cells strongly express the neuropeptide CCK (Fig. 2). CCK is expressed at varying
198 levels by many types of cortical neurons, including GABAergic and glutamatergic cells,
199 however it is particularly high in a group of GABAergic interneurons known as "CCK-
200 CB1R interneurons" or "CCK basket cells" that have been described in the hippocampus
201 and L2/3 of the neocortex (33, 39, 59, 67, 68). Although much less abundant than other
202 GABAergic interneurons in the neocortex, they are of special interest because of their
203 unique synaptic properties (67, 69, 70). In particular, these cells express CB1 cannabinoid
204 receptors in their presynaptic terminals that mediate a phenomenon known as
205 depolarization-induced suppression of inhibition (DSI) (71, 72). Depolarization of a
206 connected pyramidal cell leads to the production of endocannabinoids by the latter that
207 are transported retrogradely to the presynaptic terminals of the CCK basket cells, where
208 they bind to the CB1 receptors in the terminal, leading to suppression of GABA release
209 (73-75).

210 To test the hypothesis that non-LS Id2 neurons include "CCK basket cells", we first
211 examined the effect of depolarization of a pyramidal cell on the PSP generated on L2/3
212 PCs by light stimulation of Id2 neurons expressing the ChR CatCh (Id2-CreER; Dlx5/6-
213 Flpe; Ai80; Fig. 4A-C). Depolarization of the PC reduced the synaptic response by ~20%,
214 and this reduction was prevented by application of the CB1 receptor antagonist AM251
215 (Fig. 4B-C) suggesting that some of the presynaptic cells innervating the cell had
216 undergone DSI. In paired recordings of L2/3 LS Id2 cells and PCs, we find that the
217 synaptic response elicited by NGFCs does not undergo DSI (n=9; Fig. 4E). In contrast, in
218 paired recordings of non-LS Id2 cells, we observed DSI in 3 out of the 5 pairs tested (Fig.

219 4E). Of the cells showing DSI, two were irregular spiking and one was bursting; of the two
220 cells that did not show DSI, one was burst spiking and the other was a putative alpha-7
221 cell. These results indicate that the suppression of GABA release observed when the
222 whole population of Id2 cells is stimulated is occurring on the terminals of the non-LS Id2
223 cells. Interestingly, the proportion of the GABAergic response elicited by light activation
224 of Id2 cells that was suppressed by depolarization of the post-synaptic PC is similar to
225 the representation of non-LS cells in the L2/3 Id2 population. These observations,
226 together with the molecular analysis, suggest that the majority of the non-LS Id2 cells are
227 "CCK basket cells" (see Discussion). The morphology of IS and BS non-LS Id2 cells was
228 similar, and quite distinct from the NGFCs, with significantly longer dendrites and a less
229 symmetrical and much less dense axonal arborization (Fig. 3C-D and S5), which
230 resembles the morphology of published CCK basket cells in the neocortex (33, 68).

231 ***In vivo* properties of Id2 INs**

232 Although NGFCs are a substantial population of GABAergic INs, particularly in the
233 superficial layers of the cortex (where they are slightly more abundant than SST INs), the
234 lack of genetic strategies to study these cells has limited the characterization of their *in*
235 *vivo* properties (see Discussion). Nevertheless, given their broad output connectivity,
236 these neurons are likely to contribute significantly to inhibition throughout the cortical
237 column. We utilized our intersectional genetics approach to express CatCh in Id2 INs
238 (Id2-CreER; Dlx/5/6-Flpe; Ai80; also see Fig. 4) in order to optogenetically identify and
239 stimulate these cells in multichannel silicon probe recordings in the posterior parietal
240 cortex and V1 of freely moving and behaving animals (Fig. 5A). Single units were isolated
241 (N = 571 units from 5 mice) and separated into putative pyramidal cells (PC), narrow

242 waveform (NW) INs and wide waveform (WW) INs (76). Id2 INs expressing CatCh were
243 distinguished from other cells adjacent to the probes by measuring their firing rates in
244 response to light stimulation (Fig. 5B). Applying stringent filtering criteria (see Methods),
245 we selected 11 Id2 INs that exhibited robustly increased firing following light stimulation
246 for further analysis (Fig. 5B-C). We then characterized the firing properties of these Id2
247 INs identified in vivo in relation to PCs and other INs. These Id2 INs exhibited WW
248 characteristics, and were readily distinguishable from NW cells, previously identified as
249 PV fast-spiking INs and some SST INs (56) (Fig. 5B and D). Consistent with this, these
250 11 Id2 INs had wider auto-correlograms than other PC and NW INs, similar to the overall
251 WW group (Fig. 5E). These results indicate that the previously described WW group (76)
252 includes an unknown proportion of Id2 INs.

253 In addition to the 11 WW Id2 INs described above, we also observed two light
254 responsive Id2 INs with narrower waveform properties, although these cells did not pass
255 the selection criteria for further analysis. We estimate that the majority of Id2 INs that
256 could be identified by optotagging in our silicon probe experiments were located in deeper
257 layers (~L3-5), where the proportion of Id2 NGFC cells is >90% (Fig. 2). Thus, we
258 tentatively conclude that the 11 Id2 WW INs we selected for analysis are NGFCs, and
259 that the Id2 cells exhibiting narrower waveform properties are likely to be non-NGFC
260 CCK+ types.

261 The firing rates of PC, NW and WW neurons varied across behavioral states,
262 typically showing lower activity during sleep (Fig. 5F). In contrast, putative Id2 NGFC INs
263 exhibited relatively consistent firing rates across all conditions, with moderately increased
264 activity during REM sleep (Fig. 5F). During NREM sleep, the cortex interleaves periods

265 of high spiking activity (up states) with transient silences (down states) (56, 77). To gain
266 insights into the nature of the firing dynamics of Id2 neurons during sleep, we aligned the
267 activity of all recorded neurons to the peak of the down state (Fig. 5G). Most of the
268 neurons decreased their activity during down states, and steadily recovered their baseline
269 activity after the down state (post-down; Fig. 5H). Putative Id2 NGFCs decreased their
270 activity during down states to a similar extent as the other cell groups, but strongly
271 increased their firing above baseline levels immediately following the termination of the
272 down state (Fig. 5H, bottom; ~4 s.d. above pre-down rate for Id2; 0.2, 0.6 and -0.03 for
273 PC, NW and WW, respectively). This rebound in activity was negatively correlated with
274 the degree of firing suppression during down states for the Id2 group (Fig. 5I), suggesting
275 that intrinsic membrane properties of the Id2 INs could be mediating, at least in part, their
276 increased activity after down states. No other neuron group showed a significant
277 correlation between down and post-down state activity, notwithstanding the considerably
278 bigger sample size (Fig. 5I). Furthermore, Id2 INs fired at an early position during the up
279 states sequences (Fig. 5J), as estimated by the normalized rank order during the detected
280 up state epochs (see Methods).

281 Finally, to understand how Id2 IN activity impacts cortical circuit dynamics *in vivo*,
282 we performed optogenetic stimulation of the Id2 IN population and analyzed which
283 fraction of putative PC, NW, or WW were suppressed (neg mod in Fig. 6A), activated (pos
284 mod) or unchanged (no mod). Light stimulation resulted in a significant decrease in firing
285 rate for about half of the population of all considered cell types (Fig. 6A), consistent with
286 the broad direct inhibition expected from NGFCs. PCs in the supra-granular layers were
287 more frequently suppressed than deeper layer PCs, while both NW and WW INs showed

288 the opposite trend. Interestingly, we also observed a slow positive activity modulation of
289 a subset of INs, and to a lesser extent PCs, following stimulation of Id2 INs (Fig. 6A;
290 darker quantiles in Fig. 6B). Positively modulated responses consistently lagged the
291 negative responses (Fig. 6B-C), suggesting an indirect disinhibitory mechanism for the
292 positive responses. Overall, we find that the recruitment of Id2 INs leads to a wide range
293 of response dynamics throughout the cortical column, including both inhibitory and to a
294 lesser extent disinhibitory effects.

295 **Discussion**

296 Initiated by the finding that fast-spiking interneurons specifically express PV (78),
297 the use of molecular markers to classify subpopulations of cortical GABAergic
298 interneurons (INs) has evolved tremendously over the last decade, particularly with the
299 advent of single-cell RNA sequencing methods to profile transcriptome diversity (13, 15,
300 17, 79). These approaches have enhanced our ability to design and implement genetic
301 strategies to label and experimentally manipulate defined populations of INs in order to
302 understand their specialized functions in cortical circuitry. However, several critical
303 issues have emerged from this body of work that require consideration. First,
304 differentially expressed genes that exhibit distinct labeling patterns as assessed by
305 immunohistochemistry (IHC) or in situ hybridization (ISH) may also be expressed at
306 lower levels in broader cell populations that escape detection with those methods. In
307 transgenic animals expressing recombinases such as Cre, labeling strategies that utilize
308 viral or genetically encoded Cre-dependent reporters typically reveal these additional
309 populations due to the lower expression threshold required for labeling with these
310 genetic methods compared to IHC or ISH. For example, expression of the marker CCK
311 as assessed by IHC or ISH has been used to identify subsets of INs with relatively high
312 levels of CCK, but the use of CCK-Cre with a genetic reporter results in much more
313 extensive labeling of INs (Fig. S6) as well as pyramidal cells. Second, the
314 developmental trajectory of marker gene expression can vary substantially, in that the
315 adult expression pattern for a particular marker may be much more restricted than its
316 cumulative expression. This appears to be the case for the marker 5HT3aR (Htr3a),
317 where expression of EGFP from a BAC transgenic mouse line labels virtually *all* non-PV

318 or SST INs (i.e., all of the CGE-derived INs), a finding that lead to the conclusion that
319 PV, SST and 5HT3aR INs account for all the INs in the neocortex (46, 47). We
320 compared labeling efficiencies obtained with a knock in Htr3a-Flpo line (30) with that of
321 an Htr3a(BAC)-Cre line (80) and the Htr3a(BAC)-EGFP line used by Lee et al., and
322 found that two copies of the Htr3a-Flpo driver could largely recapitulate the cell labeling
323 observed with the higher copy number BAC transgenic lines (Fig. S7). This result, along
324 with ISH images of Htr3a expression at embryonic and adult ages (e.g., Allen Brain
325 Atlas) is consistent with broad but transient Htr3a expression in non-PV/non-SST INs
326 that then becomes restricted to a subpopulation of these INs (81).
327 Leveraging the scRNAseq resources provided by the Allen Institute (13), we
328 identified Id2 as a marker for the vast majority of the INs that do not express PV, SST,
329 or VIP. While Id2 is also expressed in pyramidal neurons and several non-neuronal cell
330 types, we employed intersectional genetics with a pan-IN driver (Dlx5/6-Flpe) to restrict
331 labeling to Id2 INs. This labeling approach relies on the use of an Id2-CreER driver,
332 which has its own pros and cons: tamoxifen induction of cre activity in Id2 cells in P21 or
333 older animals avoids spurious cell labeling arising from developmental Id2 expression,
334 but the efficiency of CreER-mediated recombination can be highly variable from animal
335 to animal depending on the effectiveness of tamoxifen administration. Overall, in well-
336 labeled brains, we found that Id2 INs comprised ~18% of the total IN population in
337 S1BF, which is consistent with our previous estimates for the prevalence of non-
338 PV/non-SST/non-VIP INs (5). In L1, a layer consisting only of GABAergic INs, >90% of
339 which are non-PV/non-SST/non-VIP, we previously identified three distinct
340 subpopulations: NGFCs, canopy cells, and alpha-7 cells (30). Here, we find that in L2-

341 5, this fourth group of INs is mostly comprised of NGFCs (~87%), with the remainder
342 consisting of a variety of CCK+ cells. While to date NGFCs have mainly been recorded
343 in superficial layers (L1-3), here we find that NGFCs are present in all layers, including
344 deep layers, but are enriched in L2/3. On the other hand, CCK+ INs are mainly located
345 in superficial L2/3 along the border with L1 and in L6. As previously shown for the
346 5HT3aR INs (5), compared to L4-5, the proportion of Id2 INs increases in L6, where this
347 group accounts for about 15% of all INs (Fig. 1). Within the L6 Id2 population, about
348 60% were NPY+ (putative NGFCs), and about 25% were strongly CCK+, with about
349 10% unaccounted for (Fig. 2). Thus, like L1, L6 is a specialized case that merits its own
350 study to elucidate the distinct IN species that reside there.

351 The massive scale of the recent cell type survey from the Allen Institute (17)
352 offers an unprecedented look at cortical and hippocampal IN diversity, and presents the
353 opportunity to assess the expression profile of specific genes across all IN types.
354 Focusing on the "CGE" branch of interneurons, we find that Id2 expression largely
355 encompasses the "Lamp5" and "Sncg" branches of their dendrogram (Fig. S1).
356 However, it is important to note that neither Lamp5 or Sncg are uniformly expressed
357 across the different subtypes in their respective branches. In the case of Sncg, many of
358 the CCK+ subtypes within that branch express low if any *Sncg* itself (e.g., within the
359 Serpinf1 sub-branch; Fig. S1). Furthermore, there is substantial overlap with VIP in the
360 Sncg population overall (~50% of cells), but this VIP/Sncg population does not appear
361 to be well labeled using our Id2 strategy (Fig. S3), likely due to the lower levels of Id2 in
362 these cells (Fig. S1). The recent development of new drivers for Lamp5 (Lamp5-Flpo;
363 Jax #037340) and Sncg (Sncg-Flpo; Jax#034424) (82) will enable new transgenic

364 targeting approaches for these respective IN populations, but the breadth and efficiency
365 of labeling achieved with these new driver lines remain to be determined. Future work
366 will hopefully resolve how this relatively sparse but remarkably diverse CCK+ IN
367 population functions within the cortex, and whether some of these cells might relate to
368 primate-specific CCK+ IN types such as the rosehip cell (83).

369 The genetic strategies described here have also facilitated the *in vivo* recording
370 of NGFCs. Outside of L1, where NGFCs express NDNF, a gene that has been used to
371 facilitate the identification and *in vivo* recording of these neurons (84-86), recording of
372 NGFCs has been limited to blind recordings followed by post-hoc identification (87-89),
373 a very low yield approach. Here, we combined optogenetic labeling via Id2
374 intersectional genetics with silicon probe recordings to identify putative NGFCs in vivo
375 (Fig. 5). We identified 11 Id2 INs located approximately in L3-5 where the vast majority
376 (>90%) of Id2 INs are NGFCs, as defined by histology and electrophysiology (Figs. 2-4).
377 We found that these putative NGFCs have a number of unique properties, including
378 relatively constant firing rates throughout different brain states and a strong rebound in
379 activity immediately following the down state during NREM sleep. We also found that
380 optogenetic stimulation of Id2 INs produced widespread inhibition of PCs and other INs
381 and delayed their activation, suggesting that the recruitment of NGFCs might drive a
382 widespread switch in the activity of all other cortical neurons. The notable rebound in
383 NGFC activity following the down state, together with the extensive output connectivity
384 of these neurons, suggests an important role for this form of GABAergic inhibition in
385 setting the stage for new incoming information during bouts of cortical activity. Future

work will certainly continue to elucidate the function of this important but neglected GABAergic cell type in regulating cortical circuitry.

388 **Materials and Methods**

389 *Mice*

390 The following primary lines of mice were used to generate the compound transgenic
391 crosses described in this paper: Id2-CreER (Jax #016222) (51), Dlx5/6-Flpe (Jax
392 #010815) (49), NPY-hrGFP (Jax #006417) (90), Nkx2.1-Flpo (Jax #028577) (28), VIP-
393 Flpo (Jax #028578) (28), Ai65 (Jax #021875) (27), Ai80 (Jax #025109) (29), and FLTG
394 (Jax #026932) (53). The reporter lines Ai65, Ai80 and FLTG were maintained as
395 homozygous stocks prior to crossing with compound heterozygous driver lines (e.g.,
396 Id2-CreER; Dlx5/6-Flpe X Ai65 homozygous), with the resulting pups genotyped for Cre
397 and Flpe to obtain experimental animals (e.g., Id2-CreER; Dlx5/6-Flpe; Ai65).
398 Genotyping was performed on genomic DNA extracted from pup toe clippings using the
399 following primers (sequences are 5' to 3'): Cre (fwd primer: caacgagtgatgaggttcgca, rev
400 primer: cgccgcataaccagtgaaaca, product = 304 bp), Flpe (fwd primer:
401 tctttagcgcaaggggtagga, rev primer: aagcacgcttatcgctccaa, product = 312 bp) and Flpo
402 (fwd primer: ccacattcatcaactgcggc, rev primer: gggccgttcttgatagcgaa, product = 355
403 bp). To activate CreER, a stock solution of tamoxifen (Sigma T5648; dissolved in corn
404 oil at 20 mg/ml on a shaker at 55°C for several hours) was administered to P21-P35
405 animals by oral gavage (4 mg/20g mouse) 3-4x over 5-7 days. All experiments were
406 performed in accordance with protocols approved by the Department of Comparative
407 Medicine at the NYU Grossman School of Medicine.

408 *Histology*

409 To obtain brain tissue for histology, animals were transcardially perfused with 4%
410 paraformalydehyde/PBS (diluted from a 32% stock; Electron Microscopy Sciences

411 cat#15714) and the brain dissected, with a post-dissection fix period of 0-16 hrs. For the
412 preparation of thin cryosections, brains were equilibrated in 30% sucrose/PBS overnight
413 before freezing in mounting medium (Tissue-Plus O.C.T. compound; Scigen 4583). For
414 the quantification of Id2 vs non-Id2 interneurons in Fig. 1, vibratome sections (50 μm)
415 were generated following perfusion/PBS washes using a Leica vibratome (VT1000S).
416 Brain cryosections (20 μm) were generated using a Leica CM3050 cryostat, collected
417 on glass slides (Shandon ColorFrost Plus; ThermoScientific cat#9991013), and stored
418 at -20°C. For immunohistochemistry (IHC), tissue sections were washed in PBS,
419 blocked for 1 hour at room temperature with PBS/0.1% Triton-X 100/2% normal donkey
420 serum, incubated overnight at 4°C with primary antibody (rabbit anti-CCK; Frontier
421 Institute cat#Af350) in blocking solution, washed in PBS, incubated 1 hour at RT with
422 secondary antibodies (for CCK IHC: donkey anti-rabbit AlexaFluor-488; Invitrogen
423 cat#A-21206). Fluorescence *in situ* hybridization for NPY and tdTomato (Fig. 2A-B) was
424 performed as described previously (30), with the following primers used to amplify
425 templates for labeled cRNA antisense probe synthesis: NPY fwd primer: 5'-
426 tcacagaggcacccagagc-3'; NPY rev primer (w/T7 sequence): 5'-
427 attaatacgactcactatagcggagtccagcctagtggtg-3'; tdTomato fwd: 5'-atcaaagagttcatgcgcttc-
428 3'; tdTomato rev primer (w/T7 sequence): 5'-
429 cattaatacgactcactatagggttccacgatggtgtagtcctc-3'.
430 *Slice preparation*
431 Adult transgenic mice of either sex (postnatal day range 30-120; mean age ± SEM =
432 46.6 ± 1.5) were terminally anesthetized with isoflurane, and once unresponsive, were
433 perfused with ice-cold sucrose-ACSF containing the following (in mM): 87 NaCl, 75

434 sucrose, 2.5 KCl, 26 $NaHCO_3$, 1.25 $NaH_2PO_4$, 10 glucose, 1.0 $CaCl_2$, and 2.0 $MgCl_2$,
435 saturated with 95% $O_2$/5% $CO_2$. Next, the mice were decapitated and the brains were
436 extracted. The brain was glued to a stage, placed into a chamber filled with bubbled ice-
437 cold sucrose ACSF, and sliced into 300 µm-thick coronal sections, angled 15º towards
438 the blade, using a Leica VT1200S vibratome. The slices were incubated at 35°C for 30
439 min in the above sucrose solution or the recording-ACSF described below and then
440 transferred to room temperature for at least 1 hour before recording commenced.
441 *Electrophysiology recordings*
442 Slices were transferred to a recording chamber perfused with ACSF containing (in mM):
443 120 NaCl, 2.5 KCl, 25 $NaHCO_3$, 1.4 $NaH_2PO_4$, 21 glucose, 0.4 Na-Ascorbate, 2 Na-
444 Pyruvate, 1 $CaCl_2$, and 2 $MgCl_2$, saturated with 95% $O_2$/5% $CO_2$ and maintained at 29 –
445 32°C. For some experiments, the bath solution contained the NMDA receptor blocker D-
446 AP5 (25 µM; Abcam), the AMPA receptor blocker CNQX (10 µM; Abcam), or the $GABA_B$
447 receptor blocker CGP-35348 (60 µM; Tocris). Neurons were visualized on an upright
448 Olympus microscope (BX50WI or BX51WI) using DIC and fluorescence illumination
449 from an LED power source (Mightex) for tdTomato and/or GFP. All neurons were
450 recorded in the barrel field of the primary somatosensory cortex in layers 2-5. Layers
451 were identified visually under DIC optics using several features. The L1-2 border was
452 marked by a sharp increase in soma density from L1. The L3-4 border was identified
453 under 4x power by the top of the barrels, the presence of horizontal fibers under 40x (in
454 L4), and the absence of pyramidal cells (PCs) seen in L2/3. L5a was a clear band below
455 L4 and the L5b-6 border was determined under 40x by a sharp drop in PCs. Neurons
456 were recorded in whole-neuron patch-clamp in current clamp and voltage clamp mode

457 using an internal solution containing (in mM): 130 K-Gluconate, 10 HEPES, 1.1 EGTA,
458 2 Mg-ATP, 0.4 Na-GTP, 10 Na-phosphocreatine, and 1.5 $MgCl_2$, 0.3-0.5% biocytin, and
459 titrated with 1 M KOH to a final pH of 7.3. Glass pipettes were pulled on a horizontal
460 puller (Sutter Instruments) using borosilicate glass (inner/outer diameter 1.5 mm / 0.86
461 mm) and had resistances of 2-6 MΩ. Before gaining whole-neuron access, a gigaseal
462 was obtained, and the pipette capacitance was compensated. Access resistances were
463 monitored throughout recordings and were completely compensated. The intrinsic
464 properties of neurons with access resistances >40 MΩ were not analyzed. All data were
465 collected using a Multiclamp 700B amplifier (Molecular Devices), a Digidata digitizer
466 (1440A or 1550B series, Molecular Devices), and Clampex version (10.6 or 10.7)
467 software (Molecular Devices); data were sampled at 20 kHz and low-pass filtered at 10
468 kHz.
469 *Electrophysiological characterization and analysis*
470 A total of 178 cells were recorded. This includes a sample of 76 cells that were
471 randomly selected for patching, and this group was used to determine the proportions of
472 each type. In addition, neurons were recorded in the same Id2-CreER; Dlx5/6-Flpe;
473 Ai65 mice but recordings were biased to superficial layer 2/3 to maximize the chances
474 of obtaining non-LS Id2 INs. Lastly, a third group included cells from animals where
475 NPY cells were labeled with GFP (i.e. Id2-CreER; Dlx5/6-Flpe; Ai65; NPY-hrGFP) to
476 facilitate the identification of non-LS Id2 INs. Neurons were characterized for intrinsic
477 and active properties in current-clamp mode from a resting potential of ~-70 mV.
478 Neurons were injected with 1 s long square pulses of increasing current. Parameters
479 relating to the neuron's intrinsic and active properties were assessed as follows:

480 *First spike latency and cell type classification:* Once rheobase was determined, several
481 current steps were delivered at rheobase to characterize the behavior of the cell. The
482 recorded cells fell into three readily separable groups. The first and most numerous
483 group exhibited a single-spike at rheobase with latencies of >500 ms and were termed
484 late-spiking (LS). The second group displayed a high-frequency (>100 Hz) burst of two
485 or more APs at rheobase and were termed burst-spiking (BS). The third group of cells
486 had single spikes at rheobase with latencies of <100 ms consistent with the charging of
487 the membrane capacitance (fivefold a tau of 20 ms). These cells also exhibited irregular
488 spiking (CV of ISI: 0.112 ± 0.029 vs. 0.053 ± 0.004 in LS, p=0.0066, Mann-Whitney
489 Test, see the section below for how CV of ISI was measured) and were classified as
490 irregular-spiking (IS).
491 *Input resistance:* This was determined from Ohm's Law based on the voltage response
492 to a 150 ms long negative voltage step of typically 20 pA.
493 *Membrane time constant (τ):* This was determined by fitting an exponential decay to the
494 voltage response from 1 s long current pulses below rheobase.
495 *AP waveform properties:* To measure these properties, only the first APs from each
496 sweep were considered, as APs in neurons with initial bursts tended to widen
497 significantly for subsequent APs, and all such APs from sweeps with total AP counts
498 <50 were considered. AP threshold and peak were calculated first and then t=0 was
499 defined at the time of AP peak. AP threshold was the voltage reading when the voltage
500 derivative was 20 mV/ms. AP peak amplitude was the maximum voltage reached in the
501 2 ms after the threshold was passed. AP half-width was the time of the AP when the
502 voltage was above the midpoint between the threshold and peak. The

503 afterhyperpolarization (AHP) was calculated as the difference in voltage between the
504 AP threshold and AP reset (minimum voltage in 10 ms window after AP peak). Finally,
505 AP max and decay slopes were the maximum and minimum values for dV/dt reached in
506 the 10 ms after the threshold was passed. Parameters were calculated separately for
507 each AP and then averaged together for the mean neuronal value.
508 *Rheobase and firing rates:* Rheobase was determined to be the current step that
509 resulted in a single spike, or for bursting cells, a single burst. The firing rate was
510 measured for each voltage sweep by counting the number of spikes in the sweep and
511 taking or interpolating the value at 2 x rheobase.
512 *Spike frequency adaptation:* For LS cells, spike frequency adaptation was measured at
513 2 x rheobase and near rheobase, during the first depolarization where a spike train was
514 observed throughout the pulse (1.3 x rheobase). For IS and BS cells, the adaptation
515 index was only measured at 2 x rheobase, since near rheobase, firing was often highly
516 irregular. The adaptation index was measured as follows: For each voltage sweep
517 during which the neuron spiked at least six times (five ISIs), an exponential function,
518 $f_{adap}(t)$, was fit to the firing-rate vs. time plot. The adaptation index (AI) for that sweep
519 was defined as AI = $f_{adap}$(1000 ms) / $f_{adap}$(100 ms), and the values at 1.3 x rheobase or 2
520 x rheobase were taken or interpolated to represent adaptation for the cell.
521 *Spiking regularity:* For each voltage sweep, all inter-spike intervals (ISIs) from the last
522 500 ms of the current step were considered. The spiking regularity was measured as
523 the coefficient of variation (CV) for these ISIs, and the reported value was taken from
524 the sweeps at 2 x rheobase.
525 *DSI – optogenetics and paired recordings*

526 For optogenetics experiments, L2/3 PCs were identified visually under DIC, patched in
527 whole-cell mode, and then confirmed as PCs by a brief electrophysiological
528 characterization. Blue light (470 nm) pulses (2 ms / >100 mA) were delivered to the slice
529 using TTL-pulses to a Mightex brand LED under 40x power with the PC soma centered.
530 Optically evoked IPSCs were recorded under a voltage clamp at a holding potential of -
531 50 mV with D-AP5 and CNQX present to block glutamatergic transmission and CGP
532 35348 to block the large $GABA_B$ component of the current characteristic of NGFCs (37).
533 Cannabinoid dependence of DSI was assessed by optogenetic experiments carried out
534 in the presence of the CB1 receptor blocker AM251 (10 μM; Abcam).
535 For paired recordings, Id2 neurons were identified as tdT+ soma in the Id2-CreER;
536 Dlx5/6-Flpe; Ai65 mouse line or tdT+/GFP± somas in the Id2-CreER; Dlx5/6-Flpe; Ai65;
537 NPY-hrGFP cross. The Id2 firing pattern was briefly characterized, and the neuron was
538 tagged as late-spiking (LS), irregular-spiking (IS), or burst-spiking (BS). A nearby PC
539 was also patched (Id2-PC inter-soma distance range 10-130 μm, average distance ±
540 SEM = 53 ± 4), and connectivity to the Id2 cell was assessed under voltage-clamp for
541 both cells by eliciting escape spikes from the Id2 cell and looking for the presence of
542 IPSCs in the PC at a holding voltage of -50 mV. If a connection was not seen, either a
543 new Id2-PC pair was tested, or the PC pipette was withdrawn with the Id2 neuron still
544 held, and another nearby PC was patched and tested. If a connection was identified,
545 then the DSI protocol was run as described in Figure 4.
546 *Morphology*
547 During whole-cell electrophysiological recordings, neurons were held for at least 15 min
548 with an internal solution containing ~0.4 or ~1.0% biocytin. Some slices, especially the

549 ones with neurons held close to 15 min, were retransferred to the incubation chamber to
550 allow for more biocytin diffusion inside the recorded cell. After filling, the slices were
551 fixed with 4% paraformaldehyde/PBS (diluted from a 32% stock; Electron Microscopy
552 Sciences cat#15714) for 1-7 days at 4°C. Fixed slices were then thoroughly washed
553 with PBS and left overnight at 4°C in a 0.4% streptavidin (AlexaFluor 647 conjugate;
554 Invitrogen) solution (498 µl 0.3% Triton X-100 in PBS, 2 µl streptavidin per slice). Slices
555 were then washed in PBS, mounted with Fluoromount-G (Invitrogen) on a glass
556 microscope slide, and imaged under a 40-63x oil-immersion objective using a confocal
557 microscope (Zeiss). Confocal images were then used to morphologically reconstruct
558 neurons in three dimensions using Neurolucida. In a few cases, cells were
559 juxtacellularly labeled and processed using CUBIC before morphological reconstruction
560 (30).

561 *Silicon probe implantation and recordings*

562 Mice (N = 5, 28–35 g, 3–10 months old) were implanted with 64-site silicon probes
563 (NeuroNexus, Cambridge NeuroTech or Diagnostic Biochips) in the PPC (AP 2.0 mm,
564 ML 1.75mm, DL 0.6mm), as described previously (56). Ground and reference wires
565 were implanted in the skull above the cerebellum, and a grounded copper mesh hat was
566 constructed, protecting, and electrically shielding, the probes. Probes were mounted on
567 plastic microdrives that were advanced to layer 6 over the course of 5–8 d after surgery.
568 A 100–200-µm fiber optic was attached to one of the shanks of the silicon probe. After
569 implantation, animals were allowed to recover for at least 1 week and were housed
570 individually under standard conditions (71–73 °F and 40–50% relative humidity) in the
571 animal facility and kept on a 12-h reverse light/dark cycle. We recorded the mice while

572 they slept or walked around freely in the home cage, and the recording session started
573 1-2 hr after the onset of the dark phase. Electrophysiological data were acquired using
574 an Intan RHD2000 system (Intan Technologies LLC) digitized with a 30 kHz rate. The
575 wide-band signal was downsampled to 1.25 kHz and used as the LFP signal. For
576 optogenetic tagging of specific neuron types, blue laser light (450 nm, Osram) pulses
577 were delivered in the PPC/V1. The maximum light power at the tip of the optic fiber was
578 1–4 mW. 100-ms light pulses with 70% of the maximum power were delivered (n = 500–
579 1,000 times at each intensity at 400 ± 200-ms random intervals).
580 *Unit activity analysis*
581 Spike sorting was performed semi-automatically with KiloSort 1
582 (https://github.com/cortex-lab/KiloSort), as previously described (56) and using our own
583 pipeline KilosortWrapper (a wrapper for KiloSort, DOI;
584 https://github.com/brendonw1/KilosortWrapper). This was followed by manual
585 adjustment of the waveform clusters using the software Phy 2
586 (https://github.com/kwikteam/phy) and plugins for phy designed in the laboratory
587 (https://github.com/petersenpeter/phy-plugins). Unit clustering generated three clearly
588 separable groups based on their spike autocorrelograms, waveform characteristics and
589 firing rate (76). Pyramidal cell (PC), narrow waveform (NW) INs and wide waveform
590 interneurons (WW) were tentatively separated based on these two clusters. A more
591 reliable cell identity was assigned after inspection of all features, assisted by
592 monosynaptic excitatory and inhibitory interactions between simultaneously recorded,
593 well-isolated units and light responses (56, 91). Units were defined as optogenetically
594 responsive cells based on the combination of three criteria

595 (https://github.com/valegarman/hippoCookBook): (1) an average firing response higher
596 than 2SD, (2) significant modulation using a p-value cutoff of $10^{-3}$ (45) and (3) against
597 randomly shuffled pulse times (500 replicates) and testing for significant difference
598 between the observed value and the random distribution. To calculate the layer identity
599 of the units, we aligned depth profiles of electrophysiological landmarks. These included
600 the largest amplitude peak of high-frequency LFP power (500 Hz–5 kHz) corresponding
601 to mid-layer 5 and four prominent sinks and sources from the averaged down–up
602 current-source density (CSD) maps for each animal, as previously described (56).
603 Rank-order estimation was used to identify the position of units repeating consistently
604 across up events. The timing from multiple units recorded simultaneously was
605 transformed in a normalized sequence order from 0 to 1 within an up event. The rate
606 centroid from each unit in an up event was considered for the rank order.
607 Brain state scoring was performed as previously described (56, 91, 92) with the
608 MATLAB resource SleepScoreMaster (https://github.com/valegarman/hippoCookBook).
609 Briefly, spectrograms were constructed with a 1-s sliding 10-s window FFT of 1250 Hz
610 data at log-spaced frequencies between 1 and 100 Hz. Three types of signals were
611 used for state scoring: broadband LFP, narrowband theta frequency LFP, and
612 electromyogram (EMG). For broadband LFP signal, principal components analysis
613 (PCA) was applied to the z-transformed (1-100 Hz) spectrogram. The first principal
614 components in all cases were based on power in the low (< 20 Hz) frequency range and
615 had negatively weighted power in the higher (> 32 Hz) frequencies. The state scoring
616 algorithm was performed by a series of divisions with thresholds set at the trough
617 between the peaks of distributions in these three metrics. After automated brain state

618 scoring, all states were manually reviewed by the experimenter. The awake-sleep index
619 was estimated as ($rate^{Awake}$ - $rate^{Sleep}$)/ ($rate^{Awake}$ + $rate^{Sleep}$), where $rate^{Awake}$ is the
620 average between the firing rate during Run and Quiet, and $rate^{Sleep}$ was the average
621 between REM sleep and NREM sleep.

622 *Statistical analysis*

623 Statistical analyses were performed with standard MATLAB functions or GraphPad
624 Prism. No specific analysis was used to estimate a minimal population sample, but the
625 number of animals, trials, in vitro and in vivo recorded cells were larger or similar to
626 those employed in previous works (91). All data presented were obtained from
627 experimental replicates with at least four independent experimental repeats for each
628 assay. All attempts of replication were successful. Data collection was not performed
629 blinded to the subject conditions. Data analysis was performed blinded to the scorer or
630 did not require manual scoring. Unless otherwise noted, for all tests, non-parametric
631 two-tailed Wilcoxon's paired signed-rank test and Kruskal-Wallis one-way analysis of
632 variance were used. For multiple comparisons, Tukey's honesty post hoc test was
633 employed, and the corrected *$P < 0.05$, **$P < 0.01$, ***$P < 0.001$ are indicated. P-values
634 for Spearman's correlations are computed using a Student's t distribution for a
635 transformation of the correlation. Results are displayed as median +/- 25th/75th
636 percentiles, unless indicated otherwise. Dispersion represents ± IC95.

637 **Acknowledgements**

638 This work was supported by NIH grants P01NS074972 and R01NS110079 (PI: BR),

639 and U19NS107616 (PI: GB).

640

641 **Author contributions**

642 Conceptualization: RM and BR; Methodology: RM, SD, MV; Formal analysis: SD, MV,

643 JM; Investigation: RM, SD, MV, IK, HZ, JH, YH, BS; Resources: GB, BR; Writing: RM,

644 MV, SD, BR; Visualization: RM, MV, SD, HZ, JH, YH; Supervision: RM, BR; Funding

645 acquisition: GB, BR.

646

647 **Declaration of interests**

648 The authors declare no competing interests.

649 **References**


650 1. Garcia-Munoz M, Arbuthnott GW. Basal ganglia-thalamus and the "crowning enigma".
651 Front Neural Circuits. 2015;9:71.
652 2. D'Souza RD, Burkhalter A. A Laminar Organization for Selective Cortico-Cortical
653 Communication. Front Neuroanat. 2017;11:71.
654 3. Ibrahim LA, Schuman B, Bandler R, Rudy B, Fishell G. Mining the jewels of the cortex's
655 crowning mystery. Curr Opin Neurobiol. 2020;63:154-61.
656 4. Schuman B, Dellal S, Pronneke A, Machold R, Rudy B. Neocortical Layer 1: An Elegant
657 Solution to Top-Down and Bottom-Up Integration. Annu Rev Neurosci. 2021;44:221-52.
658 5. Tremblay R, Lee S, Rudy B. GABAergic Interneurons in the Neocortex: From Cellular
659 Properties to Circuits. Neuron. 2016;91(2):260-92.
660 6. Feldmeyer D, Qi G, Emmenegger V, Staiger JF. Inhibitory interneurons and their circuit
661 motifs in the many layers of the barrel cortex. Neuroscience. 2018;368:132-51.
662 7. Huang ZJ, Paul A. The diversity of GABAergic neurons and neural communication
663 elements. Nat Rev Neurosci. 2019;20(9):563-72.
664 8. Fishell G, Kepecs A. Interneuron Types as Attractors and Controllers. Annu Rev Neurosci.
665 2020;43:1-30.
666 9. Jiang X, Wang G, Lee AJ, Stornetta RL, Zhu JJ. The organization of two new cortical
667 interneuronal circuits. Nat Neurosci. 2013;16(2):210-8.
668 10. Jiang X, Shen S, Cadwell CR, Berens P, Sinz F, Ecker AS, et al. Principles of connectivity
669 among morphologically defined cell types in adult neocortex. Science. 2015;350(6264):aac9462.
670 11. Taniguchi H, He M, Wu P, Kim S, Paik R, Sugino K, et al. A resource of Cre driver lines for
671 genetic targeting of GABAergic neurons in cerebral cortex. Neuron. 2011;71(6):995-1013.
672 12. Pfeffer CK, Xue M, He M, Huang ZJ, Scanziani M. Inhibition of inhibition in visual cortex:
673 the logic of connections between molecularly distinct interneurons. Nat Neurosci.
674 2013;16(8):1068-76.
675 13. Tasic B, Menon V, Nguyen TN, Kim TK, Jarsky T, Yao Z, et al. Adult mouse cortical cell
676 taxonomy revealed by single cell transcriptomics. Nat Neurosci. 2016;19(2):335-46.
677 14. Paul A, Crow M, Raudales R, He M, Gillis J, Huang ZJ. Transcriptional Architecture of
678 Synaptic Communication Delineates GABAergic Neuron Identity. Cell. 2017;171(3):522-39 e20.
679 15. Tasic B, Yao Z, Graybuck LT, Smith KA, Nguyen TN, Bertagnolli D, et al. Shared and
680 distinct transcriptomic cell types across neocortical areas. Nature. 2018;563(7729):72-8.
681 16. Gouwens NW, Sorensen SA, Baftizadeh F, Budzillo A, Lee BR, Jarsky T, et al. Integrated
682 Morphoelectric and Transcriptomic Classification of Cortical GABAergic Cells. Cell.
683 2020;183(4):935-53 e19.
684 17. Yao Z, van Velthoven CTJ, Nguyen TN, Goldy J, Sedeno-Cortes AE, Baftizadeh F, et al. A
685 taxonomy of transcriptomic cell types across the isocortex and hippocampal formation. Cell.
686 2021;184(12):3222-41 e26.
687 18. Hu H, Gan J, Jonas P. Interneurons. Fast-spiking, parvalbumin(+) GABAergic
688 interneurons: from cellular design to microcircuit function. Science. 2014;345(6196):1255263.
689 19. Inan M, Anderson SA. The chandelier cell, form and function. Curr Opin Neurobiol.
690 2014;26:142-8.

691 20. Lu J, Tucciarone J, Padilla-Coreano N, He M, Gordon JA, Huang ZJ. Selective inhibitory
692 control of pyramidal neuron ensembles and cortical subnetworks by chandelier cells. Nat
693 Neurosci. 2017;20(10):1377-83.
694 21. Gallo NB, Paul A, Van Aelst L. Shedding Light on Chandelier Cell Development,
695 Connectivity, and Contribution to Neural Disorders. Trends Neurosci. 2020;43(8):565-80.
696 22. Riedemann T. Diversity and Function of Somatostatin-Expressing Interneurons in the
697 Cerebral Cortex. Int J Mol Sci. 2019;20(12).
698 23. Lee S, Kruglikov I, Huang ZJ, Fishell G, Rudy B. A disinhibitory circuit mediates motor
699 integration in the somatosensory cortex. Nat Neurosci. 2013;16(11):1662-70.
700 24. Pi HJ, Hangya B, Kvitsiani D, Sanders JI, Huang ZJ, Kepecs A. Cortical interneurons that
701 specialize in disinhibitory control. Nature. 2013;503(7477):521-4.
702 25. Keller AJ, Dipoppa M, Roth MM, Caudill MS, Ingrosso A, Miller KD, et al. A Disinhibitory
703 Circuit for Contextual Modulation in Primary Visual Cortex. Neuron. 2020;108(6):1181-93 e8.
704 26. Kullander K, Topolnik L. Cortical disinhibitory circuits: cell types, connectivity and
705 function. Trends Neurosci. 2021;44(8):643-57.
706 27. Madisen L, Garner AR, Shimaoka D, Chuong AS, Klapoetke NC, Li L, et al. Transgenic mice
707 for intersectional targeting of neural sensors and effectors with high specificity and
708 performance. Neuron. 2015;85(5):942-58.
709 28. He M, Tucciarone J, Lee S, Nigro MJ, Kim Y, Levine JM, et al. Strategies and Tools for
710 Combinatorial Targeting of GABAergic Neurons in Mouse Cerebral Cortex. Neuron.
711 2016;91(6):1228-43.
712 29. Daigle TL, Madisen L, Hage TA, Valley MT, Knoblich U, Larsen RS, et al. A Suite of
713 Transgenic Driver and Reporter Mouse Lines with Enhanced Brain-Cell-Type Targeting and
714 Functionality. Cell. 2018;174(2):465-80 e22.
715 30. Schuman B, Machold RP, Hashikawa Y, Fuzik J, Fishell GJ, Rudy B. Four Unique
716 Interneuron Populations Reside in Neocortical Layer 1. J Neurosci. 2019;39(1):125-39.
717 31. Kisvarday ZF, Gulyas A, Beroukas D, North JB, Chubb IW, Somogyi P. Synapses, axonal
718 and dendritic patterns of GABA-immunoreactive neurons in human cerebral cortex. Brain.
719 1990;113 ( Pt 3):793-812.
720 32. Kawaguchi Y, Kubota Y. Physiological and morphological identification of somatostatin-
721 or vasoactive intestinal polypeptide-containing cells among GABAergic cell subtypes in rat
722 frontal cortex. J Neurosci. 1996;16(8):2701-15.
723 33. Galarreta M, Erdelyi F, Szabo G, Hestrin S. Electrical coupling among irregular-spiking
724 GABAergic interneurons expressing cannabinoid receptors. J Neurosci. 2004;24(44):9770-8.
725 34. Bodor AL, Katona I, Nyiri G, Mackie K, Ledent C, Hajos N, et al. Endocannabinoid
726 signaling in rat somatosensory cortex: laminar differences and involvement of specific
727 interneuron types. J Neurosci. 2005;25(29):6845-56.
728 35. Tamas G, Lorincz A, Simon A, Szabadics J. Identified sources and targets of slow
729 inhibition in the neocortex. Science. 2003;299(5614):1902-5.
730 36. Olah S, Komlosi G, Szabadics J, Varga C, Toth E, Barzo P, et al. Output of neurogliaform
731 cells to various neuron types in the human and rat cerebral cortex. Front Neural Circuits.
732 2007;1:4.

733 37. Oláh S, Fule M, Komlosi G, Varga C, Baldi R, Barzo P, et al. Regulation of cortical
734 microcircuits by unitary GABA-mediated volume transmission. Nature. 2009;461(7268):1278-
735 81.
736 38. Overstreet-Wadiche L, McBain CJ. Neurogliaform cells in cortical circuits. Nat Rev
737 Neurosci. 2015;16(8):458-68.
738 39. Galarreta M, Erdelyi F, Szabo G, Hestrin S. Cannabinoid sensitivity and synaptic
739 properties of 2 GABAergic networks in the neocortex. Cereb Cortex. 2008;18(10):2296-305.
740 40. Wamsley B, Fishell G. Genetic and activity-dependent mechanisms underlying
741 interneuron diversity. Nat Rev Neurosci. 2017;18(5):299-309.
742 41. Hu JS, Vogt D, Sandberg M, Rubenstein JL. Cortical interneuron development: a tale of
743 time and space. Development. 2017;144(21):3867-78.
744 42. Lim L, Mi D, Llorca A, Marin O. Development and Functional Diversification of Cortical
745 Interneurons. Neuron. 2018;100(2):294-313.
746 43. Gelman DM, Martini FJ, Nobrega-Pereira S, Pierani A, Kessaris N, Marin O. The
747 embryonic preoptic area is a novel source of cortical GABAergic interneurons. J Neurosci.
748 2009;29(29):9380-9.
749 44. Xu Q, Tam M, Anderson SA. Fate mapping Nkx2.1-lineage cells in the mouse
750 telencephalon. J Comp Neurol. 2008;506(1):16-29.
751 45. Liodis P, Denaxa M, Grigoriou M, Akufo-Addo C, Yanagawa Y, Pachnis V. Lhx6 activity is
752 required for the normal migration and specification of cortical interneuron subtypes. J
753 Neurosci. 2007;27(12):3078-89.
754 46. Lee S, Hjerling-Leffler J, Zagha E, Fishell G, Rudy B. The largest group of superficial
755 neocortical GABAergic interneurons expresses ionotropic serotonin receptors. J Neurosci.
756 2010;30(50):16796-808.
757 47. Rudy B, Fishell G, Lee S, Hjerling-Leffler J. Three groups of interneurons account for
758 nearly 100% of neocortical GABAergic neurons. Dev Neurobiol. 2011;71(1):45-61.
759 48. Mayer C, Hafemeister C, Bandler RC, Machold R, Batista Brito R, Jaglin X, et al.
760 Developmental diversification of cortical inhibitory interneurons. Nature. 2018;555(7697):457-
761 62.
762 49. Miyoshi G, Hjerling-Leffler J, Karayannis T, Sousa VH, Butt SJ, Battiste J, et al. Genetic
763 fate mapping reveals that the caudal ganglionic eminence produces a large and diverse
764 population of superficial cortical interneurons. J Neurosci. 2010;30(5):1582-94.
765 50. Kubota Y, Shigematsu N, Karube F, Sekigawa A, Kato S, Yamaguchi N, et al. Selective
766 coexpression of multiple chemical markers defines discrete populations of neocortical
767 GABAergic neurons. Cereb Cortex. 2011;21(8):1803-17.
768 51. Rawlins EL, Clark CP, Xue Y, Hogan BL. The Id2+ distal tip lung epithelium contains
769 individual multipotent embryonic progenitor cells. Development. 2009;136(22):3741-5.
770 52. Metzger D, Clifford J, Chiba H, Chambon P. Conditional site-specific recombination in
771 mammalian cells using a ligand-dependent chimeric Cre recombinase. Proc Natl Acad Sci U S A.
772 1995;92(15):6991-5.
773 53. Plummer NW, Evsyukova IY, Robertson SD, de Marchena J, Tucker CJ, Jensen P.
774 Expanding the power of recombinase-based labeling to uncover cellular diversity.
775 Development. 2015;142(24):4385-93.

776 54. Tricoire L, Pelkey KA, Daw MI, Sousa VH, Miyoshi G, Jeffries B, et al. Common origins of
777 hippocampal Ivy and nitric oxide synthase expressing neurogliaform cells. J Neurosci.
778 2010;30(6):2165-76.
779 55. Krienen FM, Goldman M, Zhang Q, R CHDR, Florio M, Machold R, et al. Innovations
780 present in the primate interneuron repertoire. Nature. 2020;586(7828):262-9.
781 56. Valero M, Viney TJ, Machold R, Mederos S, Zutshi I, Schuman B, et al. Sleep down state-
782 active ID2/Nkx2.1 interneurons in the neocortex. Nat Neurosci. 2021;24(3):401-11.
783 57. Chittajallu R, Pelkey KA, McBain CJ. Neurogliaform cells dynamically regulate
784 somatosensory integration via synapse-specific modulation. Nat Neurosci. 2013;16(1):13-5.
785 58. Neske GT, Patrick SL, Connors BW. Contributions of diverse excitatory and inhibitory
786 neurons to recurrent network activity in cerebral cortex. J Neurosci. 2015;35(3):1089-105.
787 59. Freund TF, Katona I. Perisomatic inhibition. Neuron. 2007;56(1):33-42.
788 60. Freund TF. Interneuron Diversity series: Rhythm and mood in perisomatic inhibition.
789 Trends Neurosci. 2003;26(9):489-95.
790 61. Kawaguchi Y, Kubota Y. GABAergic cell subtypes and their synaptic connections in rat
791 frontal cortex. Cereb Cortex. 1997;7(6):476-86.
792 62. Hestrin S, Armstrong WE. Morphology and physiology of cortical neurons in layer I. J
793 Neurosci. 1996;16(17):5290-300.
794 63. Wozny C, Williams SR. Specificity of synaptic connectivity between layer 1 inhibitory
795 interneurons and layer 2/3 pyramidal neurons in the rat neocortex. Cereb Cortex.
796 2011;21(8):1818-26.
797 64. Kawaguchi Y. Physiological subgroups of nonpyramidal cells with specific morphological
798 characteristics in layer II/III of rat frontal cortex. J Neurosci. 1995;15(4):2638-55.
799 65. Kubota Y, Karube F, Nomura M, Gulledge AT, Mochizuki A, Schertel A, et al. Conserved
800 properties of dendritic trees in four cortical interneuron subtypes. Sci Rep. 2011;1:89.
801 66. Zhou FM, Hablitz JJ. Morphological properties of intracellularly labeled layer I neurons in
802 rat neocortex. J Comp Neurol. 1996;376(2):198-213.
803 67. Glickfeld LL, Scanziani M. Distinct timing in the activity of cannabinoid-sensitive and
804 cannabinoid-insensitive basket cells. Nat Neurosci. 2006;9(6):807-15.
805 68. De-May CL, Ali AB. Cell type-specific regulation of inhibition via cannabinoid type 1
806 receptors in rat neocortex. J Neurophysiol. 2013;109(1):216-24.
807 69. Hefft S, Jonas P. Asynchronous GABA release generates long-lasting inhibition at a
808 hippocampal interneuron-principal neuron synapse. Nat Neurosci. 2005;8(10):1319-28.
809 70. Armstrong C, Soltesz I. Basket cell dichotomy in microcircuit function. J Physiol.
810 2012;590(4):683-94.
811 71. Pitler TA, Alger BE. Postsynaptic spike firing reduces synaptic GABAA responses in
812 hippocampal pyramidal cells. J Neurosci. 1992;12(10):4122-32.
813 72. Wagner JJ, Alger BE. Increased neuronal excitability during depolarization-induced
814 suppression of inhibition in rat hippocampus. J Physiol. 1996;495 ( Pt 1)(Pt 1):107-12.
815 73. Wilson RI, Kunos G, Nicoll RA. Presynaptic specificity of endocannabinoid signaling in the
816 hippocampus. Neuron. 2001;31(3):453-62.
817 74. Wilson RI, Nicoll RA. Endogenous cannabinoids mediate retrograde signalling at
818 hippocampal synapses. Nature. 2001;410(6828):588-92.

819 75. Ohno-Shosaku T, Maejima T, Kano M. Endogenous cannabinoids mediate retrograde
820 signals from depolarized postsynaptic neurons to presynaptic terminals. Neuron.
821 2001;29(3):729-38.
822 76. Petersen PC, Siegle JH, Steinmetz NA, Mahallati S, Buzsaki G. CellExplorer: A framework
823 for visualizing and characterizing single neurons. Neuron. 2021;109(22):3594-608 e2.
824 77. Steriade M, McCormick DA, Sejnowski TJ. Thalamocortical oscillations in the sleeping
825 and aroused brain. Science. 1993;262(5134):679-85.
826 78. Kawaguchi Y, Kubota Y. Correlation of physiological subgroupings of nonpyramidal cells
827 with parvalbumin- and calbindinD28k-immunoreactive neurons in layer V of rat frontal cortex. J
828 Neurophysiol. 1993;70(1):387-96.
829 79. Zeisel A, Munoz-Manchado AB, Codeluppi S, Lonnerberg P, La Manno G, Jureus A, et al.
830 Brain structure. Cell types in the mouse cortex and hippocampus revealed by single-cell RNA-
831 seq. Science. 2015;347(6226):1138-42.
832 80. Gerfen CR, Paletzki R, Heintz N. GENSAT BAC cre-recombinase driver lines to study the
833 functional organization of cerebral cortical and basal ganglia circuits. Neuron. 2013;80(6):1368-
834 83.
835 81. Pronneke A, Witte M, Mock M, Staiger JF. Neuromodulation Leads to a Burst-Tonic
836 Switch in a Subset of VIP Neurons in Mouse Primary Somatosensory (Barrel) Cortex. Cereb
837 Cortex. 2020;30(2):488-504.
838 82. Dudok B, Klein PM, Hwaun E, Lee BR, Yao Z, Fong O, et al. Alternating sources of
839 perisomatic inhibition during behavior. Neuron. 2021;109(6):997-1012 e9.
840 83. Boldog E, Bakken TE, Hodge RD, Novotny M, Aevermann BD, Baka J, et al.
841 Transcriptomic and morphophysiological evidence for a specialized human cortical GABAergic
842 cell type. Nat Neurosci. 2018;21(9):1185-95.
843 84. Cohen-Kashi Malina K, Tsivourakis E, Kushinsky D, Apelblat D, Shtiglitz S, Zohar E, et al.
844 NDNF interneurons in layer 1 gain-modulate whole cortical columns according to an animal's
845 behavioral state. Neuron. 2021;109(13):2150-64 e5.
846 85. Ibrahim LA, Huang S, Fernandez-Otero M, Sherer M, Qiu Y, Vemuri S, et al. Bottom-up
847 inputs are required for establishment of top-down connectivity onto cortical layer 1
848 neurogliaform cells. Neuron. 2021;109(21):3473-85 e5.
849 86. Abs E, Poorthuis RB, Apelblat D, Muhammad K, Pardi MB, Enke L, et al. Learning-Related
850 Plasticity in Dendrite-Targeting Layer 1 Interneurons. Neuron. 2018;100(3):684-99 e6.
851 87. Sakalar E, Klausberger T, Lasztoczi B. Neurogliaform cells dynamically decouple neuronal
852 synchrony between brain areas. Science. 2022;377(6603):324-8.
853 88. Fuentealba P, Klausberger T, Karayannis T, Suen WY, Huck J, Tomioka R, et al. Expression
854 of COUP-TFII nuclear receptor in restricted GABAergic neuronal populations in the adult rat
855 hippocampus. J Neurosci. 2010;30(5):1595-609.
856 89. Klausberger T, Magill PJ, Marton LF, Roberts JD, Cobden PM, Buzsaki G, et al. Brain-
857 state- and cell-type-specific firing of hippocampal interneurons in vivo. Nature.
858 2003;421(6925):844-8.
859 90. van den Pol AN, Yao Y, Fu LY, Foo K, Huang H, Coppari R, et al. Neuromedin B and
860 gastrin-releasing peptide excite arcuate nucleus neuropeptide Y neurons in a novel transgenic
861 mouse expressing strong Renilla green fluorescent protein in NPY neurons. J Neurosci.
862 2009;29(14):4622-39.

863 91. Valero M, Navas-Olive A, de la Prida LM, Buzsaki G. Inhibitory conductance controls
864 place field dynamics in the hippocampus. Cell Rep. 2022;40(8):111232.
865 92. Watson BO, Levenstein D, Greene JP, Gelinas JN, Buzsaki G. Network Homeostasis and
866 State Dynamics of Neocortical Sleep. Neuron. 2016;90(4):839-52.
867

# Fig. 1: Id2 expression delineates a fourth major group of INs

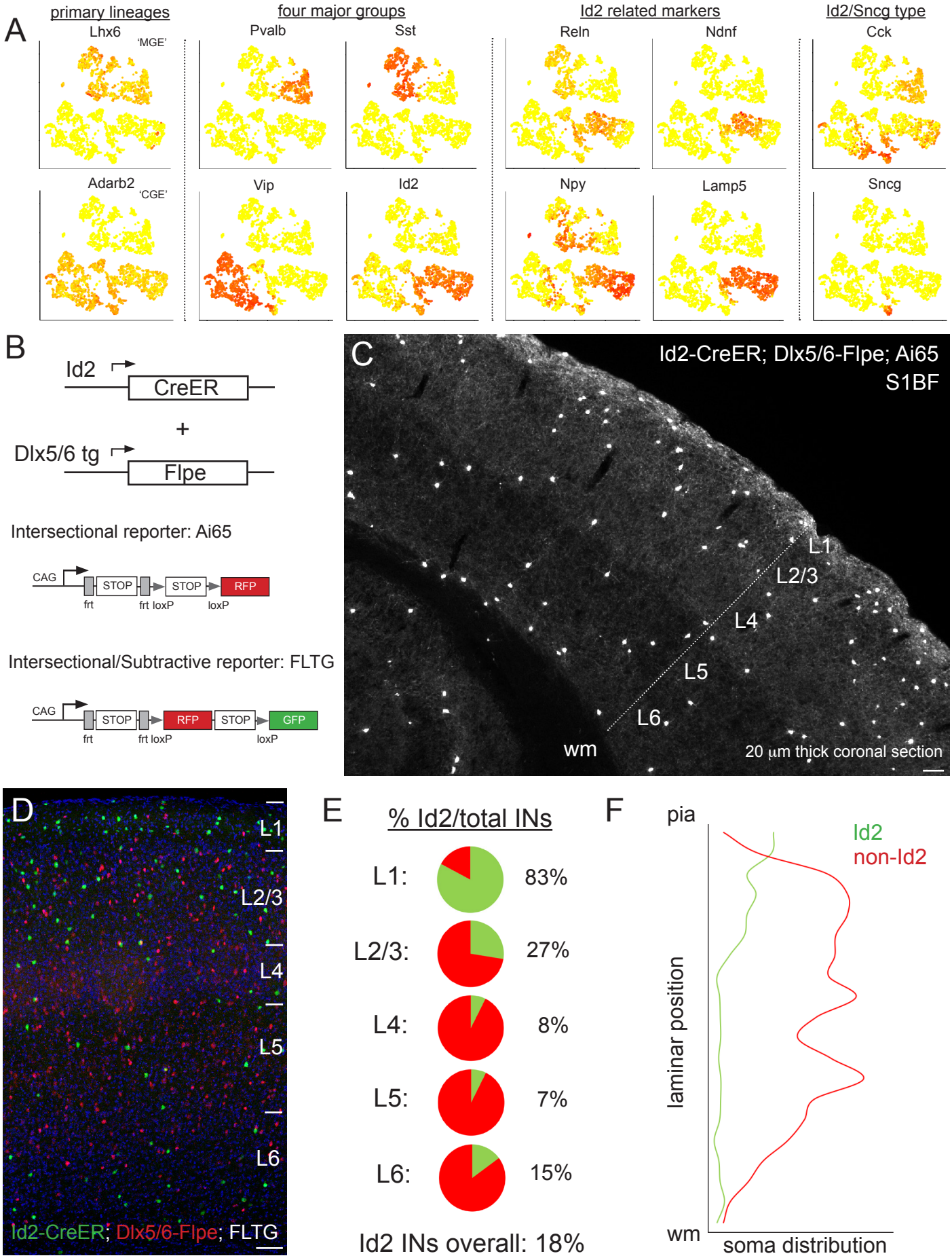

**Figure 1: Id2 expression delineates a fourth major group of INs**.

(**A**) Public scRNAseq data (from Tasic et al., 2016; comprised of ~ 3000 INs purified from the visual cortex, with transcriptome diversity represented as tSNE plots; see Mayer et al., 2018) underlying the hypothesis that the non-VIP CGE IN population can be distinguished by the expression of *Id2*. Primary IN lineages originating from the medial (MGE) and caudal (CGE) ganglionic eminences express *Lhx6* and *Adarb2*, respectively. To a first approximation, MGE-derived INs are comprised of parvalbumin (*Pvalb*) and somatostatin (*Sst*) subtypes, whereas CGE-derived INs consist of vasoactive intestinal peptide (*Vip*) and inhibitor of DNA binding 2 (*Id2*) subtypes. Expression of the marker genes Reelin (*Reln*), neuron-derived neurotrophic factor (*Ndnf*), neuropeptide Y (*Npy*) and cholecystokinin (*Cck*) is evident within the Id2 population, which roughly corresponds to the lysosomal associated membrane protein 5 (*Lamp5*) plus synuclein-γ (*Sncg*) IN categories in Tasic et al., 2016. (**B**) Intersectional genetic strategies for targeting Id2 INs. The Id2-CreER knock in driver line combined with the Dlx5/6-Flpe transgenic line allows for labeling of Id2 INs with tdTomato when crossed with the Ai65 intersectional reporter (or the channelrhodopsin CatCh when crossed with Ai80). The use of the intersectional/subtractive reporter FLTG enables the dual color labeling of Id2 and non-Id2 INs. (**C**) Image of coronal cryosection (20 μm thick) of an Id2-CreER; Dlx5/6-Flpe; Ai65 labeled brain (P30) reveals the distribution of Id2 INs throughout the layers of the cortical S1 barrel field (S1BF). (**D**) Image of a coronal field in S1BF of Id2-CreER; Dlx5/6-Flpe; FLTG labeled brain with Id2 INs in green and non-Id2 INs in red. (**E**) Proportion of Id2 vs. non-Id2 INs across the layers of S1BF determined from cell counts of the cross in (D). Id2 INs comprise 18% of the

overall IN population (3812 cells counted across 4 brains). (**F**) Distribution of Id2 and non-Id2 IN somas across S1BF lamina. Scale bars in panels C and D represent 100 μm.

**Fig. 2: Histological analysis of Id2 INs (S1BF)**

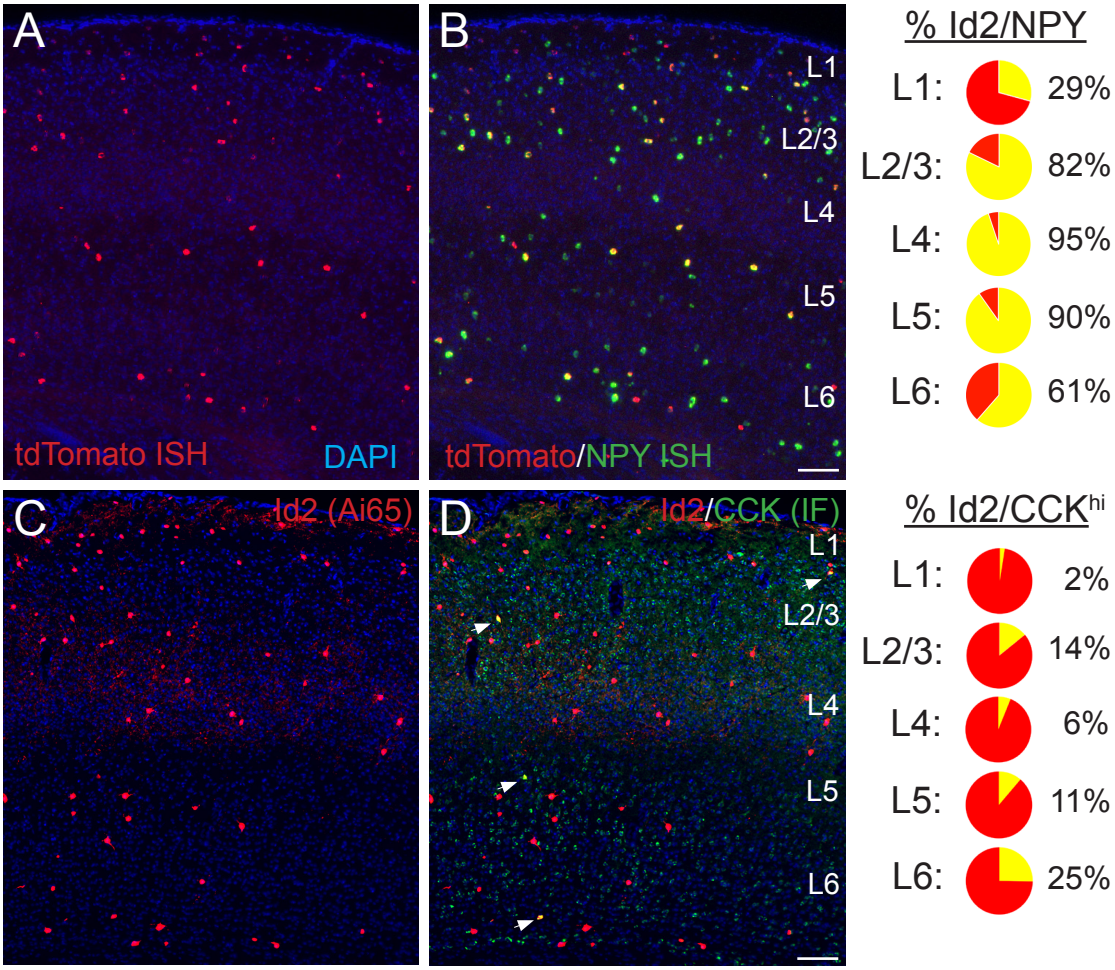

**Figure 2: Histological analysis of Id2 INs in S1BF.**

(**A-B**) Assessment of *Npy* expression in Id2 INs (Id2-CreER; Dlx5/6-Flpe; Ai65). Fluorescent *in situ* hybridization (FISH) with cRNA probes for *tdTomato* (red; panel A) and *Npy* (green; both red and green channels shown in panel B) mRNAs on brain cryosections (20 μm thick) reveals that outside of L1, the vast majority of Id2 INs express *Npy* (L2-5: 87%). The percentages of Id2/*Npy* cells (yellow) in each layer are represented as pie charts on the right. (**C-D**) Assessment of CCK expression in Id2 INs (Id2-CreER; Dlx5/6-Flpe; Ai65). Immunofluorescent histochemistry (IHC) for tdTomato (red; panel A) and CCK (green) reveals that a fraction (15%) of Id2 cells in L2-6 express high levels of CCK ($CCK^{hi}$), with the highest proportion of Id2/CCK cells observed in L2 and L6. The percentages of Id2/CCK cells (yellow) in each layer are represented as pie charts on the right. Scale bars in panels B and D represent 100 μm.

## Fig. 3: Electrophysiology and morphology of Id2 INs in S1BF

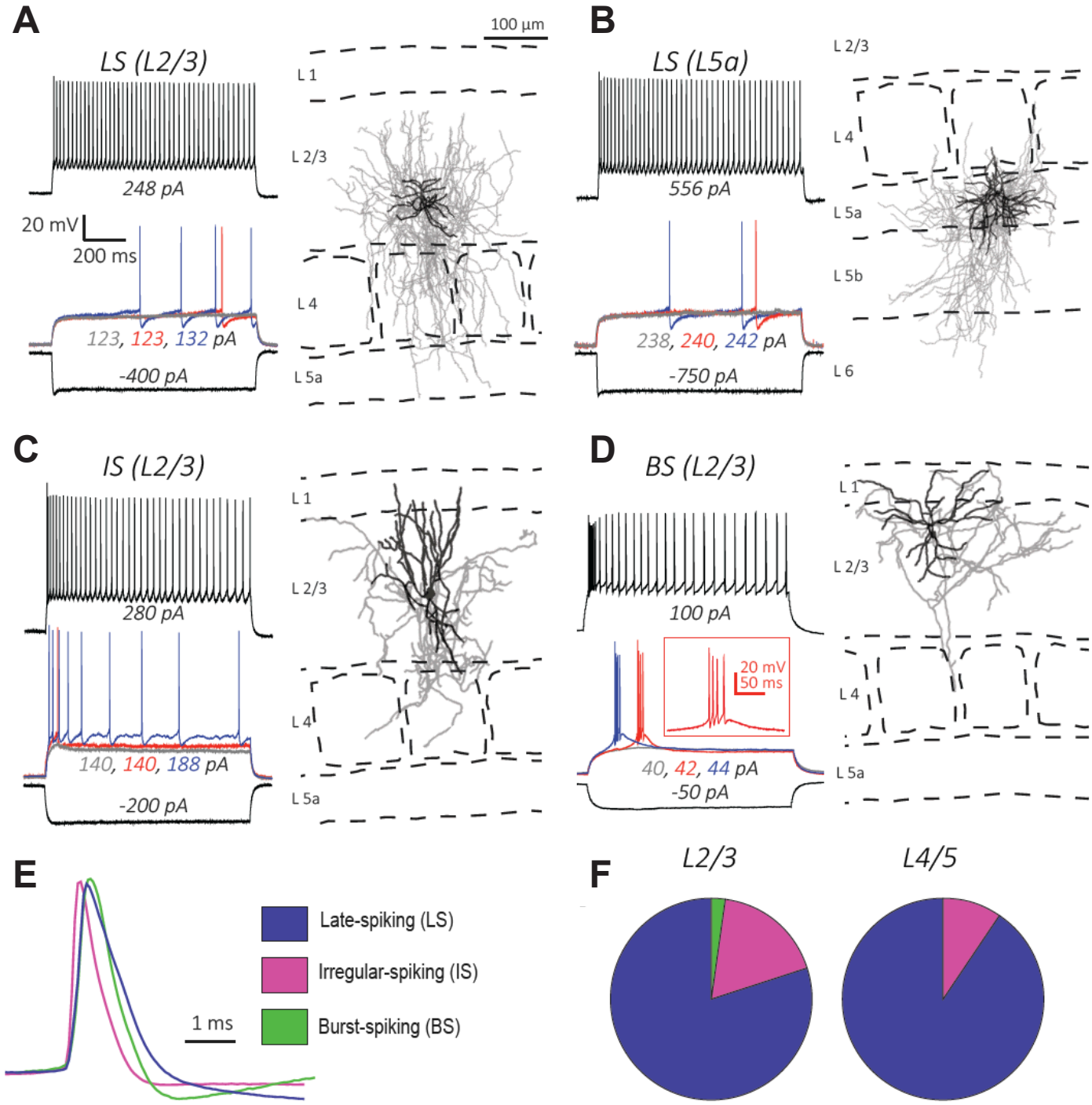

**Figure 3. Electrophysiology and morphology of Id2 INs in S1BF.** (**A-D**) Four examples of the types of cells encountered in this survey and their respective locations in the cortical column: **(A-B)** Late-spiking (LS), **(C)** Irregular-spiking (IS), and **(D)** Burst-spiking (BS). For electrophysiological characterization, cells were injected with current to bring them to -70 mV. Each voltage trace shows the response of the cell to a 1s long current injection at the indicated levels which are: i) a negative current to hyperpolarize the cell to -100 mV [black-lower trace], ii) current steps just below [grey trace], at [blue trace], and just above rheobase [red trace], and iii) current at roughly double the rheobase [black-upper trace]. To the right of each cell's voltage traces is the morphological reconstruction from biocytin fills of the same recorded cell with the cortical layers and barrel fields indicated with dashed lines. Dendrites are shown in black and axons are shown in gray. (**E**) Overlay of first action potential waveforms at rheobase from the three described cell types. (**F**) Proportions of the three main cell types encountered in L2/3 and L4/5. For L2/3, 45 randomly selected cells were patched and characterized electrophysiologically. The proportions of the cell types were: 80% LS, 18% IS, and 2% BS. For L4/5, 31 randomly selected cells were characterized, and the proportions of the cell types were: 90% LS, 10% IS, and 0% BS.

## Fig. 4: The non-LS Id2 population exhibits DSI

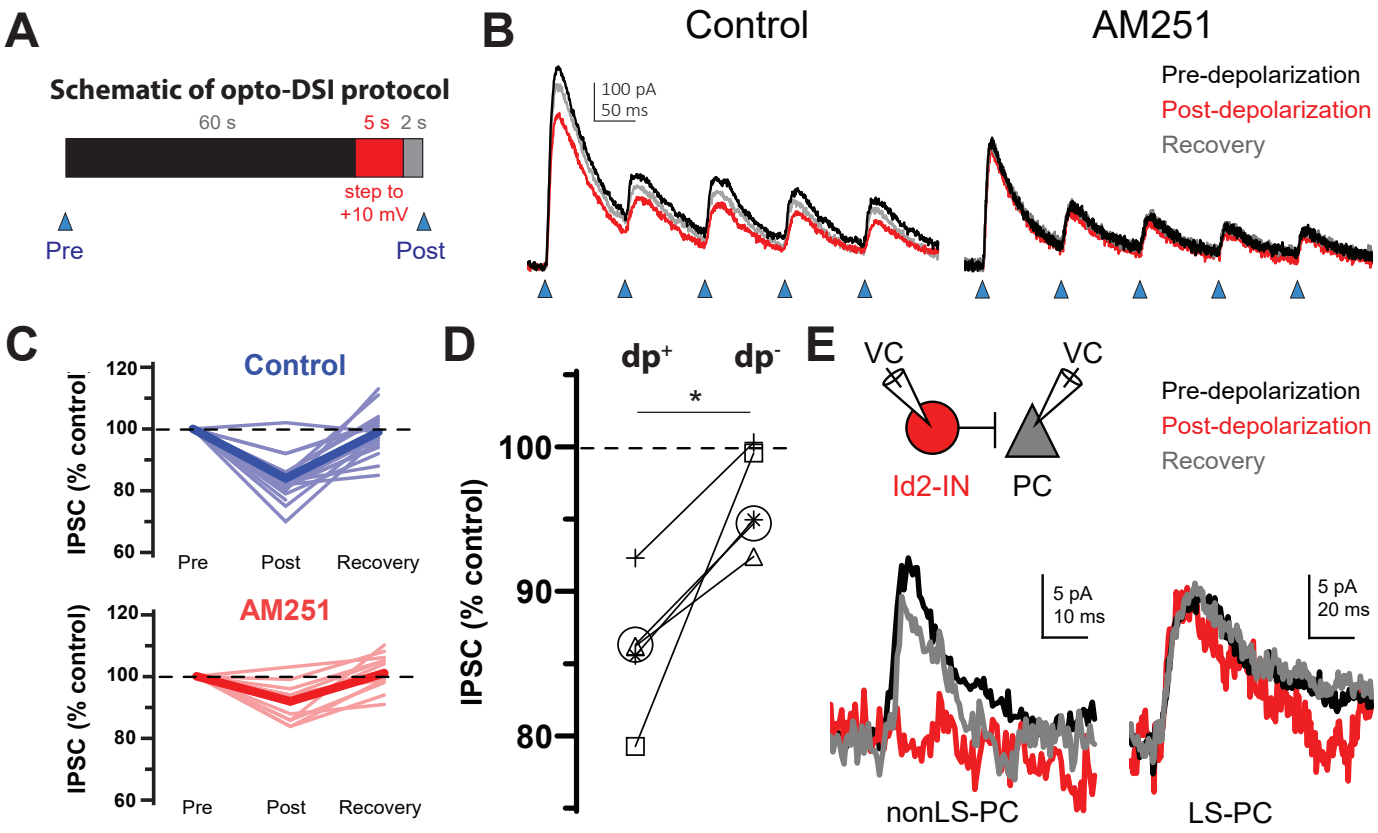

**Figure 4. The non-LS Id2 population exhibits DSI.** (**A**) Protocol used for revealing depolarization-induced suppression of inhibition (DSI). DSI was first assessed via optogenetics in L2/3 pyramidal cells (PCs) in the following manner: PCs were recorded in voltage-clamp mode in cortical slices from Id2-CreER; Dlx5/6-Flpe; Ai80 animals, in which the channelrhodopsin CatCh is widely expressed in the Id2 IN population. Control IPSCs were elicited by light pulses of 2ms in duration. Then, after a 60s interval, the PC was stepped to +10 mV for 5s, and after a 2s recovery, another IPSC was elicited in the same manner. (**B**) Sample traces from optogenetic experiments. In the drug-free condition (left panel), the peak current decreases slightly but noticeably and recovers by the next stim 60s later. However, in the presence of the CB1 receptor antagonist AM251 (10 μM) [right panel], this decrease was not observed. (**C**) Summary data from all cells tested as in (B). Thin, faint lines are the averages for each cell across three or more repetitions. Dark, solid lines are the averages across all cells. The average decrease in IPSC amplitude in the control condition was 16±2% (n = 18 cells, N = 8 animals). Two-tailed paired t-tests of Post vs. Pre and Recovery vs. Post were significant (p=1e-6, p=6e-6). The average decrease in IPSC amplitude in the AM251 condition was 8±1% (n = 11 cells, N = 4 animals). Also, the average decrease post-depolarization in Control vs. AM251 was significant by a two-tailed unpaired t-test (p=0.002). (**D**) A subset of five cells was tested in which the DSI protocol was carried out with (dp+) or without (dp-) a depolarization to +10 mV to control for variability or rundown of the synaptic current. Trials that incorporated the depolarization step exhibited significantly greater decreases in IPSC amplitude than those that lacked it (p=0.014, two-tailed paired t-test). (**E**) DSI was also detected in several nonLS-PC pairs but not in LS-PC pairs. Recording

configuration and sample current traces from two PCs: a post-synaptic PC to a nonLS cell (left) and a post-synaptic PC to an LS cell (right). Current traces represent a DSI experiment. Several probe stimuli were given to obtain a baseline average (black trace), then the depolarization step to +10 mV was delivered to the PC, and 1-2 s later, the PC was probed again (red trace). The cell was then probed several times afterwards to assess recovery (grey trace). The mouse lines used for these experiments were Id2-CreER; Dlx5/6-Flpe; Ai65 or the same with the addition of an NPY-hrGFP allele to facilitate the identification of nonLS cells. Out of 46 nonLS-PC pairs tested, only 9 (20%) were connected (compared to 24% for $CB_1IS \rightarrow P$ in Galaretta et al 2008). Out of 27 LS-PC pairs tested, 19 (70%) were connected. DSI was assessed in 9 LS-PC pairs and not observed in any of them, whereas out of 5 nonLS-PC pairs tested for DSI, 3 pairs exhibited it.

# Fig. 5: Activity of Id2 INs *in vivo*

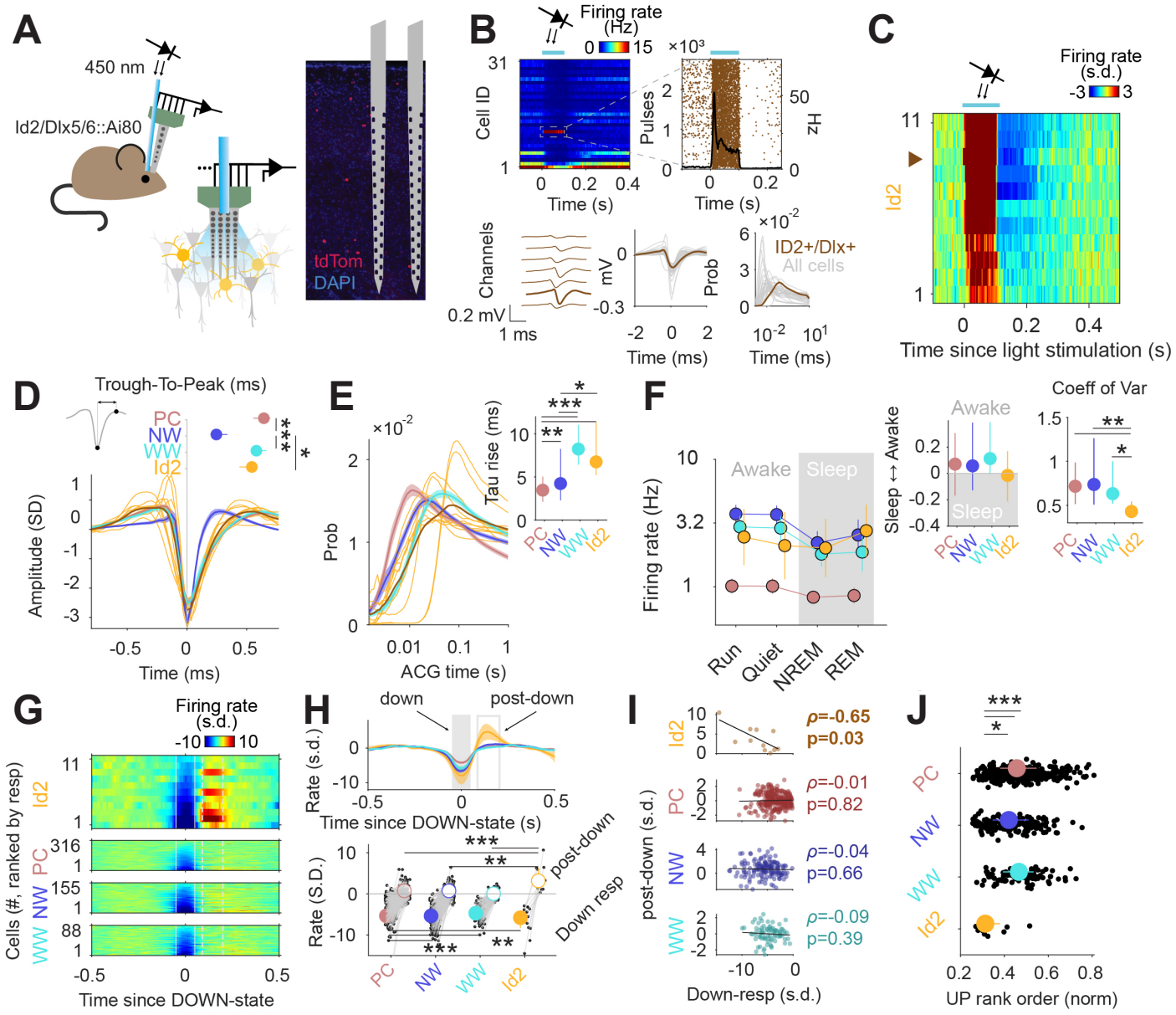

**Figure 5. Activity of Id2 INs *in vivo*.** (**A**) Schematic of the opto-tagging experiments that were used to identify Id2 INs in freely behaving mice. Combined light fiber-recording probes were implanted in Id2-CreER; Dlx5/6-Flpe; Ai80 mice. (**B**) Peristimulus time histogram (PSTH) from 31 isolated neurons from a single recording session. Note one light-responsive neuron in position 11. The peristimulus raster plot, waveform and auto-correlogram for that light-responsive Id2 IN-light responsive unit are shown in brown. All remaining cells from this session are shown in clear gray for comparison. (**C**) Peristimulus histogram (PSTH) for all isolated units classified as Id2 IN-light responsive neurons (from N = 5 mice). (**D**) Average spike waveform (mean ± 95% confidence interval (CI95)) and through-to-peak spike duration (inset; $P < 10^{-61}$, Kruskal-Wallis test) for PCs, NW INs, WW neurons and Id2 INs (N = 317 PCs, 155 NW INs and 88 WW neurons). The average waveform from all Id2 IN-light responsive neurons are overlayed in yellow. (**E**) Same as in **D** but for the average firing auto-correlogram (ACG) in log scale and time constant of the rising phase of the ACG (inset; $P < 10^{-24}$). (**F**) Median firing rates of PCs, NW INs, WW neurons, and light responsive-Id2 INs (Cell type: $F_{3,2261} = 151.44$, $P < 10^{-89}$; State: $F_{3,2261} = 10.74$, $P = 0.035$; Interaction: $F_{9,2261} = 0.97$, $P = 0.46$). Sleep to Awake index ($P = 0.051$, Kruskal-Wallis test) and coefficient of variance of the firing rate ($P = 0.034$, Kruskal-Wallis test) as insets. Sleep to Awake index was near zero only for the Id2 IN group (PC: $Z = 2.55$, $P = 0.010$; NW: $Z = 3.16$, $P = 0.002$; WW: $Z = 0.08$, $P = 0.98$; one-sample Wilcoxon signed rank test). (**G**) Peri-down state Z-scored firing histogram for light-responsive-Id2 INs (top), and all PCs, NW INs, WW neurons (middle to bottom), as ranked according to their magnitude of event response. Solid lines delimit the ±50-ms window used to estimate the unit

responses during down states. Dashed lines delimit the +90-ms to +200-ms window used to estimate the post-down state responses. Id2 INs increase their firing rate during the post-down epoch. (**H**) Temporal dynamics of the Z-scored peri-down-state responses across all groups (top; mean ± IC95). Contrary to what was observed in PCs, NW INs and WW neurons, Id2 neurons significatively increased their firing rate above baseline levels during the post-down epoch (post-down: $P < 10^{-8}$; down: $P < 10^{-15}$). (**I**) The magnitude of the post-down state response as a function of the activity during the down state events. Only Id2 neurons show a significant correlation (Spearman correlation). (**J**) Group differences of the average rank position during up state epochs ($P < 10^{-5}$, Kruskal-Wallis test). Id2 INs lead the up-state sequences.

## Fig. 6: Circuit effects of Id2 IN stimulation *in vivo*

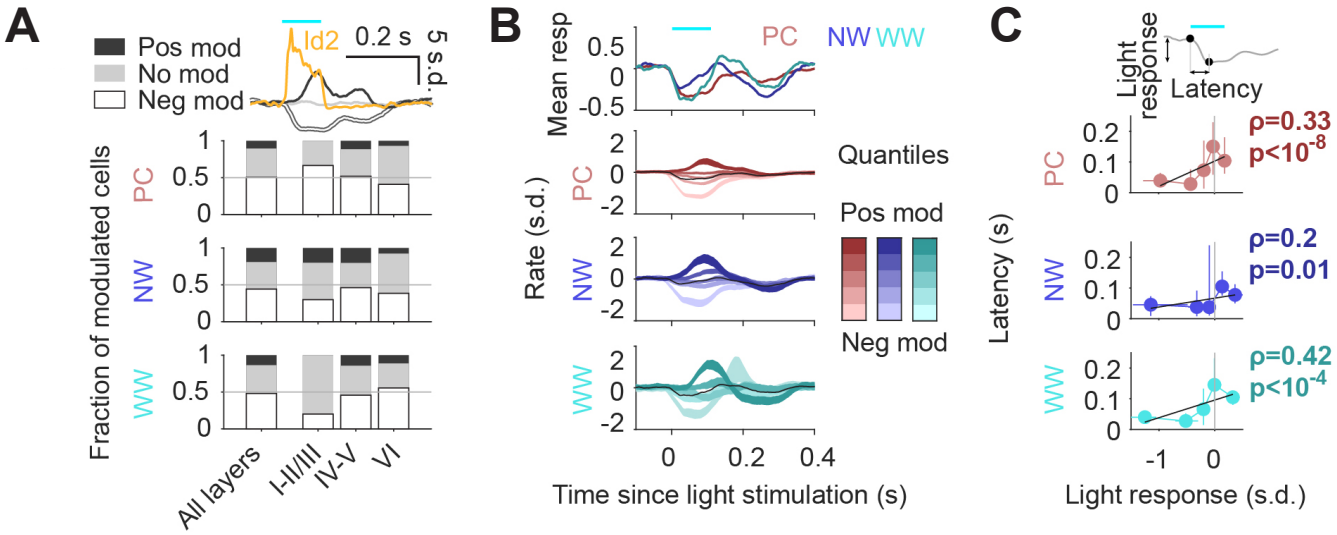

**Figure 6. Circuit effects of Id2 IN stimulation *in vivo***. (**A**) Fraction of negatively modulated (neg mod), positively modulated (pos mod), and unmodulated neurons (no mod) in the PC, NW and WW groups across cortical layers. Average peristimulus histogram for all three modes of response (pos mod, neg mod, and no mod) is shown in the top inset. (**B**) Peristimulus histograms for PCs, NW INs, and WW neurons, each separated into 5 quantiles based on their +0-ms to +100-ms average firing rate response (light to dark shades). (**C**) Peak latency for the light-evoked responses in all neuron groups as a function of the +0-ms to +100-ms rate response. Positively modulated responses peaked consistently later than negative responses (Spearman correlation).

| Electrophysiological property | LS in L2/3 (n ≥ 15) | LS in L4-5 (n ≥ 5) | IS in L2/3 (n ≥ 5) | BS in L2/3 (n ≥ 5) |
|---|---|---|---|---|
| First AP latency (ms) | 804 ± 16 | 827 ± 32 | 53 ± 4 | 143 ± 37 |
| Input Resistance (MΩ) | 188 ± 7 | 130 ± 11*** | 199 ± 32 | 301 ± 32*** |
| Membrane τ (ms) | 12 ± 0.5 | 11 ± 0.8 | 13 ± 1.2 | 17 ± 1.4** |
| AP half-width (ms) | 0.70 ± 0.02 | 0.63 ± 0.08 | 0.48 ± 0.04*** | 0.57 ± 0.05* |
| AP threshold (mV) | -35 ± 1 | -33 ± 2 | -38 ± 2 | -41 ± 2* |
| AP rise slope (mV/ms) | 283 ± 15 | 367 ± 61 | 404 ± 60 | 322 ± 46 |
| AP fall slope (mV/ms) | -84 ± 4 | -108 ± 20 | -150 ± 19*** | -135 ± 29* |
| AHP amplitude (mV) | 14.4 ± 0.5 | 12.9 ± 1.1 | 9.9 ± 0.9*** | 6.6 ± 1.3*** |
| Rheobase (pA) | 150 ± 17 | 205 ± 44 | 155 ± 18 | 51 ± 7*** |
| Firing rate (Hz) (at 2 x rheobase) | 38 ± 3 | 29 ± 4 | 40 ± 6 | 31 ± 7 |
| Firing Regularity (at 2 x rheobase) | 0.053 ± 0.004 | 0.050 ± 0.008 | 0.112 ± 0.029** | 0.262 ± 0.124** |
| Adaptation Index (near rheobase) | 1.14 ± 0.08 | 1.06 ± 0.11 | -- | -- |
| Adaptation Index (at 2 x rheobase) | 0.76 ± 0.03 | 0.72 ± 0.03 | 0.26 ± 0.05*** | 0.24 ± 0.14** |

**Table 1. Electrophysiological properties of Id2 INs in S1BF.** Values are reported as Mean ± SEM. Significance was tested for each group against LS in L2/3 using the Mann-Whitney test, * denotes significance between 0.01-0.05, ** denotes significance between 0.001-0.01, and *** denotes significance <0.001. Significance was not assessed for the first spike latency as cells were categorized on that basis. For some cells, not all of the parameters were assessed, so the n values are the minimum number of cells used to calculate all of the parameters. See Materials and Methods section for how these parameters were obtained.